Versatile Synthesis of Nano-Icosapods via Cation Exchange for Effective Photocatalytic Conversion of Biomass-Relevant Alcohols

Dan Xu,[+a] Li Zhai,[+ac] Zhangyan Mu,[a] Chen-Lei Tao,[a] Feiyue Ge,[a] Han Zhang,[b] Mengning Ding,[a] Fang Cheng,[*b] Xue-Jun Wu[*a]

[a]State Key Laboratory of Coordination Chemistry, School of Chemistry and Chemical Engineering, Nanjing University, Nanjing 210023, China

[b]State Key Laboratory for Organic Electronics and Information Displays & Jiangsu Key Laboratory for Biosensors, Institute of Advanced Materials (IAM), Jiangsu National Synergetic Innovation Center for Advanced Materials (SICAM), Nanjing University of Posts and Telecommunications, Nanjing 210023, China

[c]Department of Chemistry, City University of Hong Kong, Tat Chee Avenue, Kowloon, Hong Kong, China

[+]These authors contributed equally to this work

*Corresponding authors. E-mail: iamfcheng@njupt.edu.cn, xjwu@nju.edu.cn

Experimental Section

Chemicals. Silver nitrate ($AgNO_3$, 99.9999%), cadmium oxide (CdO, ≥99.99%), cadmium chloride ($CdCl_2$, 99.99%), sulfur powder (S, ≥99.98%), palladium(II) acetylacetonate ($Pd(acac)_2$, ≥99.99%), copper(I) iodide (CuI, ≥99.999%), oleylamine (OAm, 70%), oleic acid (OA, 90%), 1-octadecene (ODE, 90%), and trioctylphosphine (TOP, 97%) were purchased from Sigma-Aldrich. N-methylformamide (NMF, 99%), n-octadecylphosphonic acid (ODPA, 97%), n-hexylphosphonic acid (HPA, 97%), and ammonium thiocyanate (NH_4SCN, ≥98%) were bought from Alfa Aesar. Zinc(II) chloride ($ZnCl_2$, 99%), manganese(II) chloride ($MnCl_2$, 99%), nickel(II) chloride ($NiCl_2$, 99%), cobalt(II) chloride ($CoCl_2$, 99%), acetonitrile (CH_3CN, ≥99.8%), and methanol (MeOH, ≥99.9%) were purchased from Shanghai Aladdin Biochemical Technology Co., Ltd. Benzyl alcohol (BA, 99%), benzaldehyde (BZD, 99%), 4-methoxybenzyl alcohol (4-OCH_3-BA, 99%), 4-methoxybenzaldehyde (4-OCH_3-BZD, 98%), 4-methylbenzyl alcohol (4-CH_3-BA, 98%), 4-methylbenzaldehyde (4-CH_3-BZD, 98%), 4-chlorobenzyl alcohol (4-Cl-BA, 98%), 4-chlorobenzaldehyde (4-Cl-BZD 97%), furfuryl alcohol (FA, 99%), furfural (FF, 99%), 5-hydroxymethylfurfural (HMF, 99%), 2,5-diformylfuran (DFF, 98%), 2-thiophenemethanol (97%), 2-thiophenecarboxaldehyde (98%), cyclohexanemethanol (97%), cyclohexanecarboxaldehyde (97%), tetrachloromethane (CCl_4, 97%), and triethylamine (TEA, 97%) were purchased from Energy Chemical Reagent Co., Ltd. (Shanghai, China). Hexane (≥99.0%), toluene (≥99.0%), and acetone (≥99.8%) were of analytical grade and were used as received without any further purification.

Synthesis of Ag-CdS icosapods with lengths of ~45 nm. Highly monodispersed fivefold multi-twinned icosahedron Ag nanocrystals was firstly synthesized as seeds via a reported procedure and re-dispersed in 2.5 mL of TOP and finally kept in the glovebox for further use (MTAg-TOP dispersion).[1] The Ag-CdS icosapods were prepared by seeded growth method according to our recently report with slight modification.[2] Typically, 0.9 mmol of CdO (115.6 mg), 0.1 mmol of $CdCl_2$ (18.3 mg), 5 mmol of OA (1.4 g), 0.66 mmol of ODPA (219.9 mg), 1.2 mmol of HPA (199.2 mg) and 6 mL of ODE were added into a 50 mL three-neck flask and degassed at 120 ℃ for

0.5 h, and then the flask was purged with N_2. Next, the solution was heated to 280 ℃ for 45 min under nitrogen atmosphere until the solution become optically clear. Then, the mixture was heated to 300 ℃ and 0.5 mL of TOP was injected. When the temperature was recovered to 300 ℃, 0.6 mL of MTAg-TOP dispersion mixed with 0.5 mL of TOPS (prepared by dissolving 24.0 mg S in 0.5 mL of TOP) was rapidly injected into the reaction flask and allowed to proceed for 10 min. The whole reaction was performed under magnetic stirring of 800 rpm. After 10 min of reaction, the heating mantle was removed and the solution was naturally cooled down. A volume of 10 mL toluene was injected into the reaction flask when the mixture was cooled to 120 ℃. After further cooled to 60 ℃, the product was precipitated by adding 5 mL ethanol and then collected by centrifugation at 5000 rpm for 2 min, the supernatant was discarded carefully. The obtained precipitate was washed with the mixture of toluene and ethanol twice and then dispersed into toluene.

Preparation of Cu_2S icosapods via cation exchange. For transforming Ag-CdS icosapods to Cu_2S icosapods, the cation exchange reaction was carried out according to a previous report with slight modification.[3] Typically, 100 mg CuI was dissolved into mixture composed of 10 mL of CH_3CN and 2.5 mL methanol, and then 10 mg Ag-CdS icosapods dispersed in 1 mL toluene was added. The mixture was ultrasonicated for 30 min at room temperature and then centrifuged at 5000 rpm for 2 min. The cation exchange process was repeated twice to make sure that all Cd^{2+} was completely replaced by Cu^{+}. The final precipitates washed twice with CH_3CN/toluene (*v/v*, 1:5), and was re-dispersed in hexane for further use**.**

Preparation of metal sulfide MS (M=Cd, Zn, Mn, Ni, and Co) icosapods. A series of cation exchange reaction were performed following the published literatures with slight modification.[4-6] For the preparation of CdS icosapods, 0.2 mmol $CdCl_2$ (37 mg), 2 mL OAm and 5 mL ODE were added into a 50 mL three-neck flask and degassed at 100 ℃ for 0.5 h, and then the flask was purged with N_2. The mixture was heated to 180 ℃ and maintained for 30 min to form a Cd-OAm complex, followed by cooling to 150 ℃. The obtained Cu_2S icosapods (~5 mg) was suspended in 1.5 mL TOP by shaking and then injected into the reaction solution at 150 ℃. The reaction was kept at 150 ℃

for 5 min to complete the cation exchange reaction. The whole reaction was performed under magnetic stirring of 800 rpm. After the reaction, the heating mantle was removed and the reaction solution was naturally cooled to room temperature. The product was precipitated by 5 mL acetone /methanol (*v/v*, 2:3) and then collected by centrifugation at 5000 rpm for 2 min, the supernatant was discarded carefully. The obtained precipitate was washed twice with the toluene/ethanol and then dispersed into toluene.

The synthetic procedures for the preparation of other metal sulfide icosapods was analogous to that of CdS icosapods except that $ZnCl_2$, $MnCl_2$, $NiCl_2$ and $CoCl_2$ are used as the starting metal salts to replace $CdCl_2$.

Preparation of Pd_xS and CdS-Pd_xS icosapods. The Pd_xS and CdS-Pd_xS icosapods were synthesized via a previously reported method with slight modifications.[7] Typically, a specific amount of $Pd(acac)_2$ (20.0 mg for Pd_4S icosapods, and 2.0 mg for CdS-Pd_xS icosapods), 2.5 mL of OA and 8.5 mL of OAm were added into a 50 mL three-neck flask and degassed at 80 ℃ for 30 min. The solution was heated to 180 ℃ under nitrogen atmosphere. During the heating, a mixture of ~10 mg of CdS icosapods, 0.5 mL of OA, and 2 mL of OAm were rapidly injected into the reaction flask when the temperature reached 140 ℃ and then the reaction was kept at 180 ℃ for 15 min. The whole reaction was under magnetic stirring of 800 rpm. After the reaction, the heating mantle was removed and the reaction was naturally cooled. A volume of 10 mL toluene was injected into the reaction flask when the mixture was cooled to 120 ℃. After further cooled to 60 ℃, the product was precipitated by adding 2 mL ethanol and then collected by centrifugation at 5000 rpm for 2 min, the supernatant was discarded carefully. The obtained precipitate was washed twice with the toluene/ethanol and then dispersed into toluene.

Synthesis of CdS nanorods (NRs) and CdS-Pd_xS NRs. CdS NRs and CdS-Pd_xS NRs are synthesized according to a published literature.[7]

Phase transfer of as-prepared CdS-Pd_xS icosapods. 10 mg CdS-Pd_xS icosapods was dissolved in 5 mL toluene, and then 100 mg NH_4SCN dispersing in 5 mL NMF was added with vigorous stirring. After 1h stirring, the CdS-Pd_xS icosapods was transferred to NMF phase and collected by centrifugation at 13000 rpm for 5 min. The precipitate

was washed with methanol twice and dried under vacuum at room temperature for further use.

Characterizations. UV-vis measurements were collected on SHIMADZU UV-2600 spectrophotometer. Powder X-ray diffraction (XRD) patterns were recorded on Bruker D8 diffractometer with Cu Kα radiation (λ = 1.5406 Å), operated in the 2θ range of 10−80°. SEM images and SEM-EDX profiles were obtained from a field-emission scanning electron microscope JEOL JSM-7800F. TEM and HRTEM images were collected from JEOL JEM-2100 and FEI TF20 operated at 200 kV. High angle annular dark field STEM (HAADF-STEM) images and EDS maps were obtained using a FEI Titan3 G2 60-300 operated at 300 kV with double-aberration Correctors. X-ray photoelectron spectroscopy (XPS) measurements were performed on a PHI5000 Versa Probe system with a monochromatic Al Kα source and a charge neutralizer. All the binding energies were referred to the C 1s peak at 284.8 eV of the surface adventitious carbon.

Photoelectrochemical (PEC) measurements. Transient photocurrent response was conducted on an electrochemical workstation (CHI760, Shanghai Chenhua Limited, China) with a standard three-electrode system. 0.5 M Na_2SO_4 aqueous solution was served as the electrolyte for PEC measurements. 2 mg phase transferred photocatalysts (CdS-Pd_xS icosapods) dispersed in 1.0 mL ethanol was mixed with 2.5 μL Nafion solution (0.05 wt.%), and then the mixture was slowly dropped on indium tin oxide (ITO) glass (A = 0.5 cm^2), and dried in air to prepare the working electrodes. Ag/AgCl and platinum plate were adopted as reference electrode and counter electrode, respectively. A 100 W Xenon lamp with 420 nm cut-off filter was employed as visible-light irradiation source.

Transient absorption (TA) measurements. Femtosecond (fs) transient absorption spectroscopy measurements were investigated by a Pharos ultrafast Yb:KGW laser (Light Conversion) with a regenerative amplifier, which produces IR pulses (10 W) centered at 1030 nm wavelength (200 kHz, pulse width < 290 fs). A portion of this beam (80%) was sent through an optical parametric amplifier (OPA, ORPHEUS, Light

Conversion) to generate the pump beam of 400 and 550 nm for the excitation (pulse duration ~70 fs), and the residual was used as the probe beam. The resulting pump and probe pulses were directed into a TA spectrometer (Harpia, Light Conversion). Both the pump and probe pulses were sent into an optical bench. The probe pulse was focused into a sapphire crystal, generating continuum white light as the probe light. The frequency of the pump pulse was reduced to 95 Hz, using a chopper, and the absorption with and without pumping light was measured and compared. For TA measurements in the time domain of 4.8 ns, a time delay of the probe pulse with respect to the pump pulse was regulated by a computer controlled optical delay stage. Pump and probe pulses were focused and overlapped on the sample plane, which was housed in a 1 mm cuvette. The transmitting white-light probe pulses were directed into a photodiode array detector (Kymera, Andor). The resulting absorption differences were calibrated and analyzed using software (Harpia service app, Light Conversion). Samples with an optical absorbance of 1.0 in toluene were used.

Photocatalytic biomass-relevant alcohols oxidation and hydrogen (H_2) production. 10 mg CdS-Pd_xS icosapods powder photocatalyst was dispersed in 10 mL mixture of BA (10 mM) and CH_3CN, and then the mixture was ultrasonicated for 30 min to get an adsorption-desorption equilibrium under dark condition. Next, the suspension was transferred into a double walled glass reactor, and thoroughly degassed by three cycles and backfilled with nitrogen to remove the air and dissolved oxygen. Subsequently, the reactor was kept at a constant temperature (25 ℃) with water circulated through a thermostat and irradiated from the top through a quartz window with 300 W Xe lamp (Beijing Perfectlight, Microsolar 300) equipped with a 420 nm cutoff filter for 2 h under slight stirring. The light power density of the Xe lamp measured by a photoradiometer (PL-MW2000, Beijing Perfectlight Co., Ltd.) was 200 mW cm^{-2}. The evolved hydrogen was sampled periodically by a gas chromatography (Nexis GC-2030) equipped with a thermal conductive detector using argon as the carrier gas. The solution products were identified by gas chromatography spectrometry (Nexis GC-2030 with a DB-Waxetr column) equipped with a flame ionization detector using nitrogen as the

carrier gas. To identify the reactive species during the photocatalytic process, 1 mmol of triethylamine (TEA), tetrachloromethane (CCl_4), and butylated hydroxytoluene (BHT) were added as the scavengers for photoinduced holes (h^+), electrons (e^-) and carbon centered radical (•C), respectively. Conversion of biomass-relevant alcohol and selectivity of corresponding aldehyde are calculated according to the following equations (Eqs. (1)-(2)):

$$Conversion\ (\%) = \frac{C_0 - C_{alcohol}}{C_0} \times 100\% \qquad (1)$$

$$Selectivety\ (\%) = \frac{C_{aldehyde}}{C_0 - C_{alcohol}} \times 100\% \qquad (2)$$

where C_0 is the initial concentration of biomass-relevant alcohol, C_{alcohol} and C_{aldehyde} are the concentrations of biomass-relevant alcohol and corresponding aldehyde at a certain period of time after the photocatalytic reaction, respectively. The apparent quantum yield (AQY) of photocatalyst was measured with Xe lamp irradiation light through 420 nm band-pass filter (full width half maximum of 20 nm). The AQY was calculated using the following formulas:

$$AQY = \frac{N_C}{N_i} \times 100\% = \frac{2 \times r_{H_2}}{I_i} \times 100\%$$

where N_c is number of photons that are converted into products (H_2), N_i is number of incident photons, r_{H_2} is rate of H_2 generation, I_i is incident light intensity, which was determined by laser power meter (PM100D, THORLABS). For photocatalytic cycle test, the photocatalyst washed three times with CH_3CN after the photocatalytic experiment for the next round test.

***In situ* electron paramagnetic resonance (EPR) measurements.** The *in situ* EPR spectroscopic measurements were carried out at room temperature using a Bruker A300 EPR spectrometer. 10 mg CdS-Pd_xS icosapods were dispersed in a mixed solution of 10 mL CH_3CN containing 0.1 mmol BA and 0.5 mmol DMPO. After 30 min to get an adsorption-desorption equilibrium under dark condition, the suspension was injected into a glass capillary which was placed in a sealed glass tube under argon (Ar)

atmosphere. The sealed glass tube was placed in the microwave cavity of EPR spectrometer and was irradiated with Xe lamp during EPR measurements at room temperature.

Results and Discussion

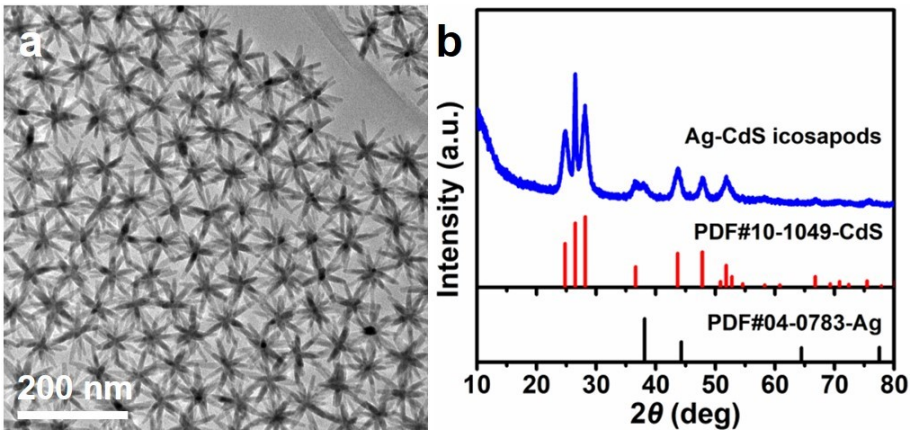

Fig. S1 (a) TEM image and (b) XRD pattern of the Ag-CdS icosapods with arm length of ~45 nm. The standard wurtzite CdS (red line, PDF#10-1049) and cubic Ag (black line, PDF#04-0783) are shown as references.

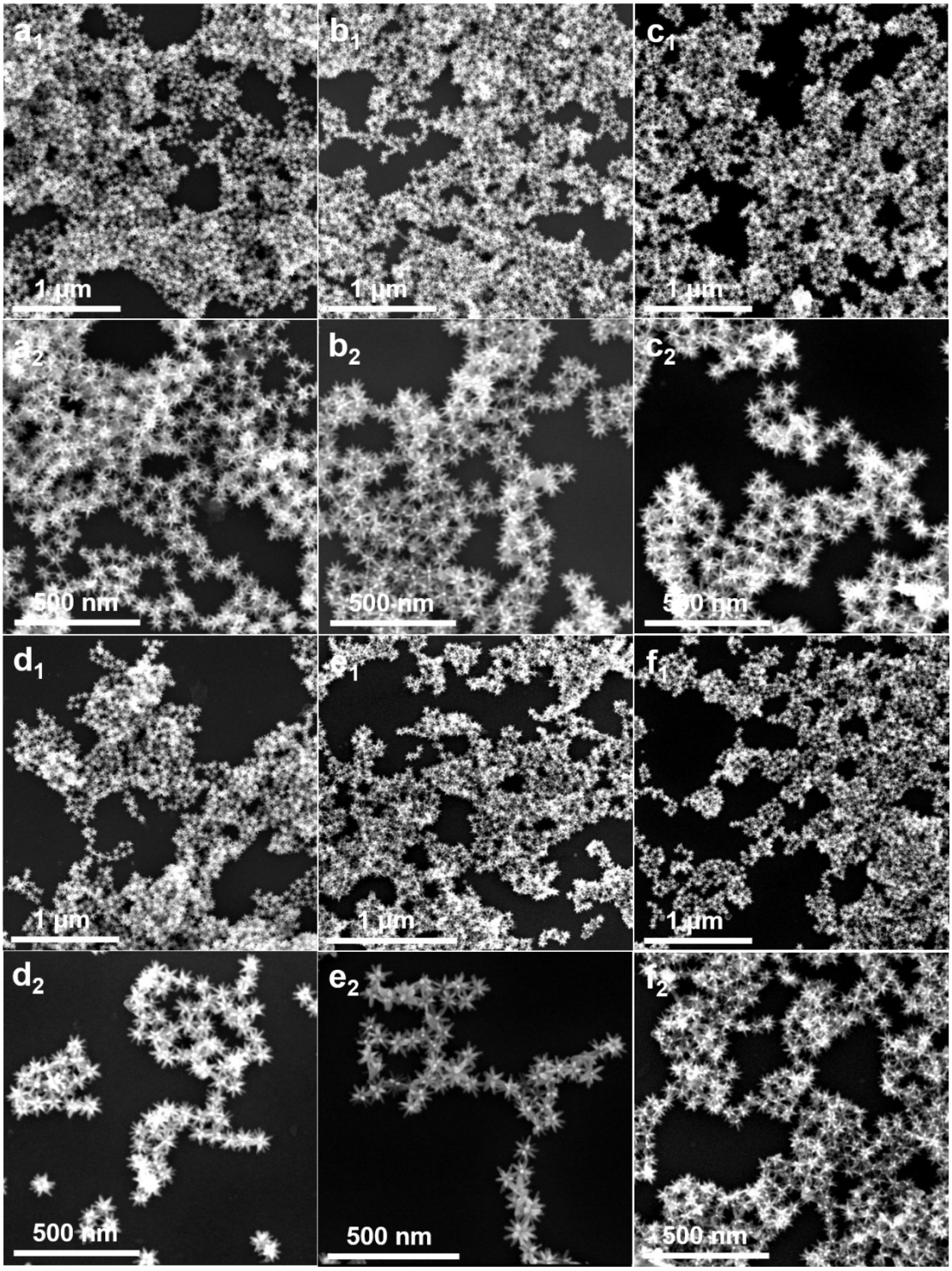

Fig. S2 SEM images of the (a_1, a_2) Cu_2S, (b_1, b_2) CdS, (c_1, c_2) ZnS, (d_1, d_2) MnS, (e_1, e_2) Co_9S_8, and (f_1, f_2) Ni_3S_4 icosapods under different magnifications.

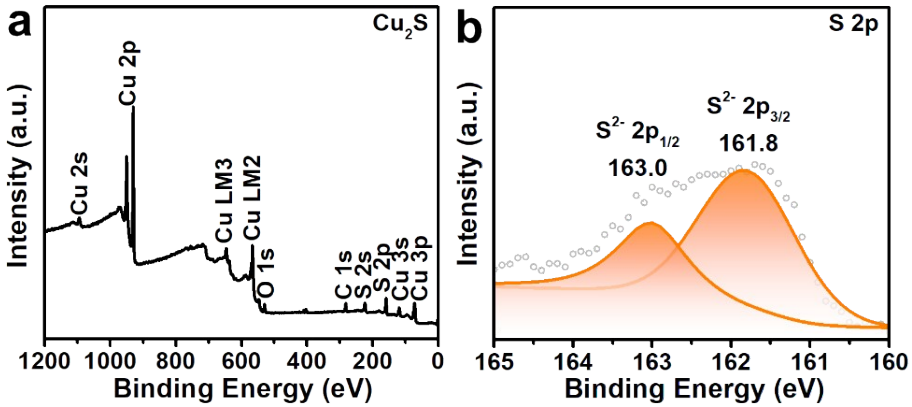

Fig. S3 (a) Survey scan XPS spectrum and (b) high-resolution XPS spectrum of S 2p for the Cu_2S icosapods.

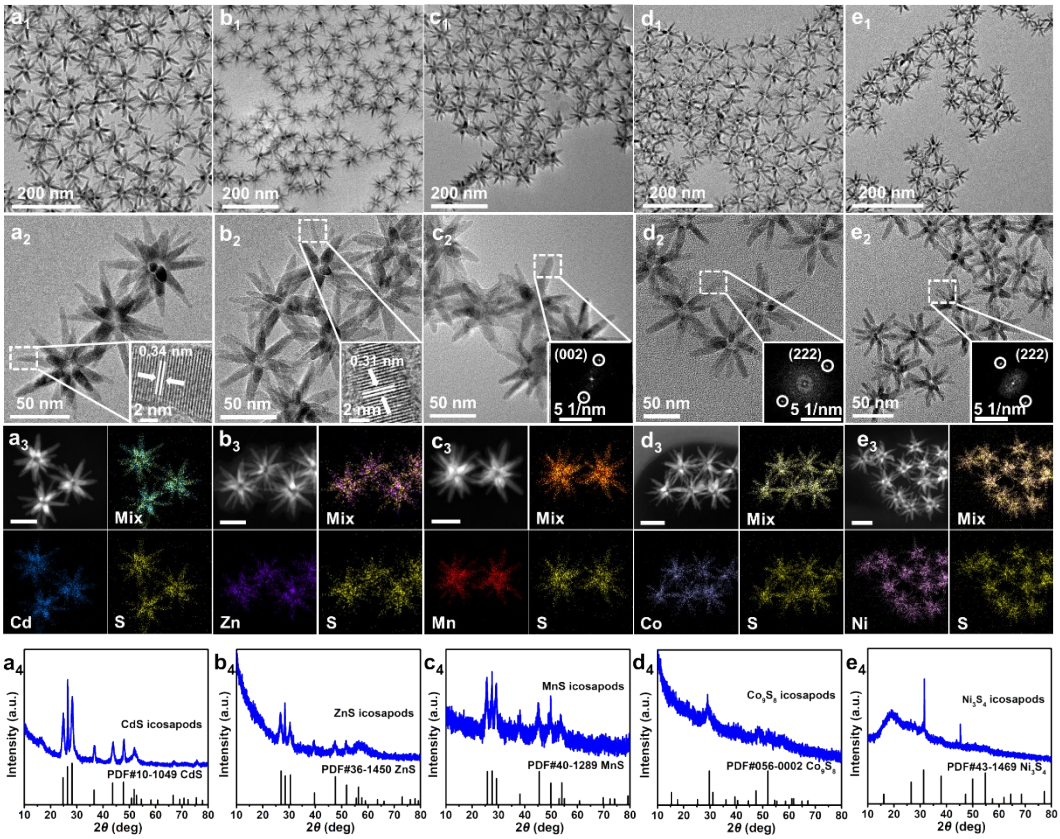

Fig. S4 (a_1-e_1) TEM images of as-prepared CdS, ZnS, MnS, Co_9S_8, and Ni_3S_4 icosapods, respectively. (a_2-e_2) HRTEM images of the CdS, ZnS, MnS, Co_9S_8, and Ni_3S_4 icosapods. Insets: HRTEM and FFT images taken from the selected area indicated by the white dotted squares. (a_3-f_3) HAADF-STEM images and corresponding EDS elemental mappings of the CdS, ZnS, MnS, Co_9S_8, and Ni_3S_4 icosapods, respectively (Scale bar, 50 nm). (a_4-f_4) XRD patterns of the corresponding icosapods. The standard diffraction peaks for wurtzite CdS (PDF#10-1049), wurtzite ZnS (PDF#36-1450), wurtzite MnS (PDF#40-1289), pentlandite Co_9S_8 (PDF#56-0002) and polydymite Ni_3S_4 (PDF#43-1469) are used as references.

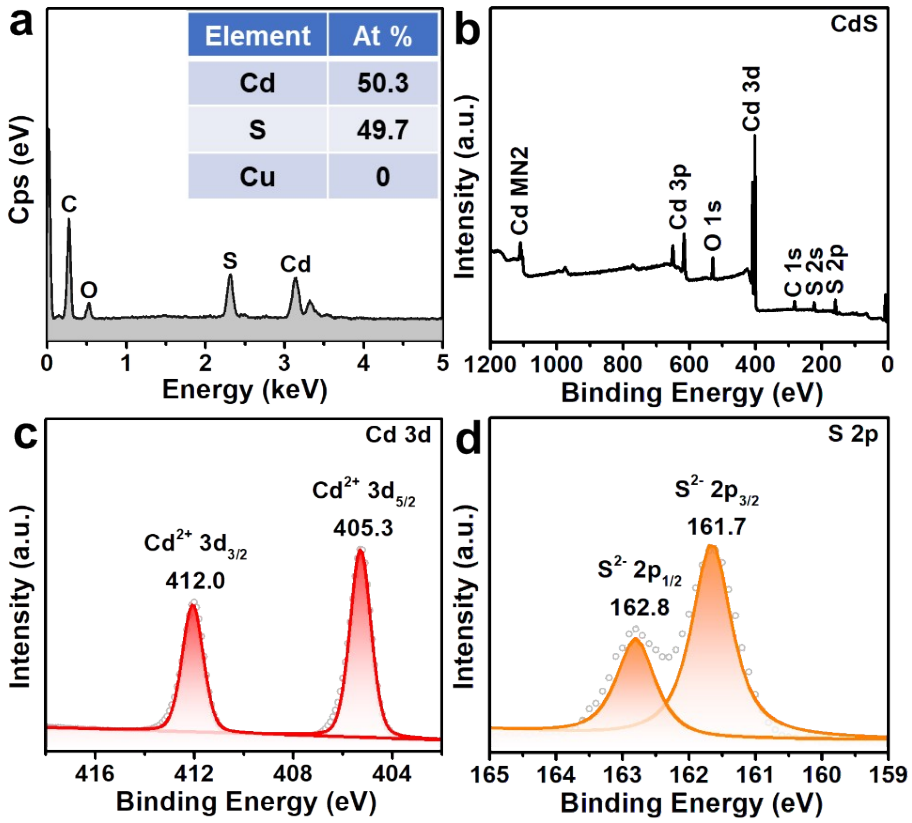

Fig. S5 (a) SEM-EDX profile and corresponding elemental contents (inset) of the synthesized CdS icosapods. (b) Survey scan XPS spectrum and high-resolution XPS spectra of (c) Cd 3d, and (d) S 2p for the CdS icosapods, respectively.

The SEM-EDX profile shows that the atomic ratio of Cd and S in the CdS icosapods is ~1.01 (Fig. S5a), which is close to the stoichiometric value of CdS, and there is no residual Cu element. Survey scan XPS spectrum shows the presence of Cd and S in the icosapods. In the high-resolution XPS spectrum of Cd 3d, the peaks located at 412.0 and 405.3 eV can be ascribed to Cd^{2+} $3d_{3/2}$ and Cd^{2+} $3d_{5/2}$ of CdS, respectively (Fig. S5c).[8] Whereas, the peaks located at 162.8 and 161.7 eV can be ascribed to S^{2-} $2p_{1/2}$ and S^{2-} $2p_{3/2}$ of sulfides for CdS, respectively (Fig. S5d).[8]

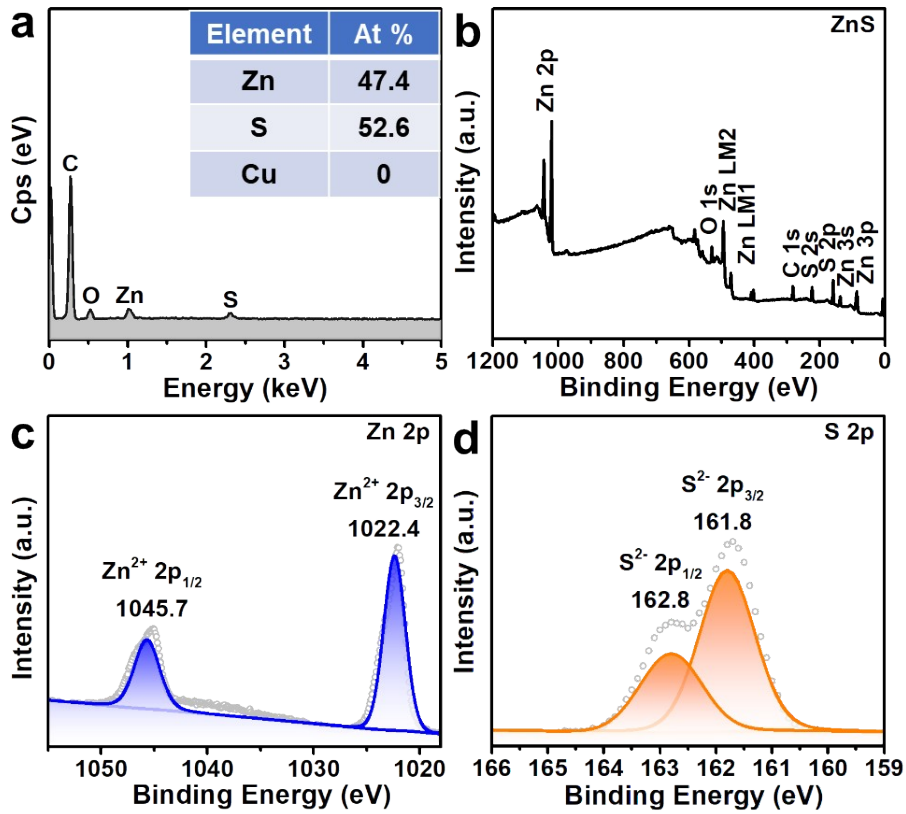

Fig. S6 (a) SEM-EDX profile and corresponding elemental contents (inset) of the synthesized ZnS icosapods. (b) Survey scan XPS spectrum and high-resolution XPS spectra of (c) Zn 2p, and (d) S 2p for the ZnS icosapods, respectively.

The SEM-EDX profile shows that the atomic ratio of Zn and S in the ZnS icosapods is ~0.90 (Fig. S6a), which is close to the stoichiometric value of ZnS, and there is no residual Cu element. The survey scan XPS spectrum demonstrates the coexistence of Zn and S in the icosapods (Fig. S6b). The peaks located at 1045.7 and 1022.4 eV can be ascribed to Zn^{2+} $2p_{1/2}$ and Zn^{2+} $2p_{3/2}$ of ZnS, respectively (Fig. S6c).[9,10] Whereas, the peaks located at 162.8 and 161.8 eV can be assigned to S^{2-} $2p_{1/2}$ and S^{2-} $2p_{3/2}$ of sulfides for ZnS, respectively (Fig. S6d).[9,10]

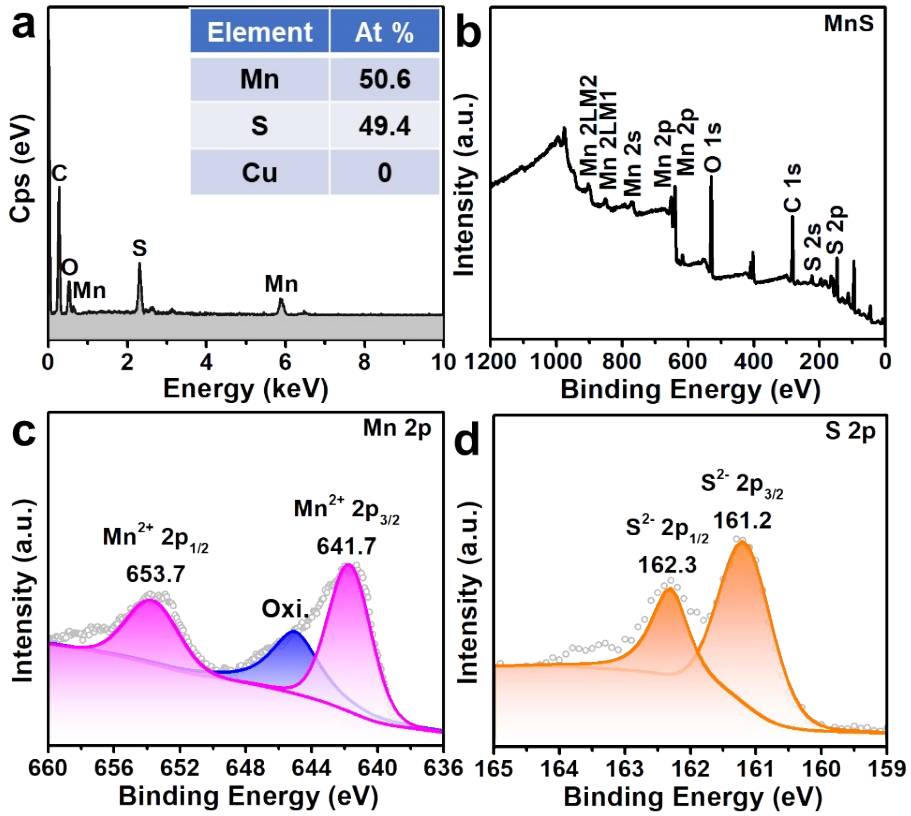

Fig. S7 (a) SEM-EDX profile and corresponding elemental contents (inset) of the synthesized MnS icosapods. (b) Survey scan XPS spectrum and high-resolution XPS spectra of (c) Mn 2p, and (d) S 2p for the MnS icosapods, respectively.

The SEM-EDX profile shows that the atomic ratio of Mn and S in the MnS icosapods is ~1.02 (Fig. S7a), which is close to the stoichiometric value of MnS, and there is no residual Cu element. As shown in Fig. S7b, the survey scan XPS spectrum also reveals the presence of Mn and S in the icosapods. The peaks located at 653.7 and 641.7 eV can be ascribed to Mn^{2+} $2p_{1/2}$ and Mn^{2+} $2p_{3/2}$ of MnS, respectively (Fig. S7c).[11] Notably, a shoulder peaked at 645.0 eV may be consigned the existence of Mn–O bonding resulting from surface slight oxidation of Mn(II) oxide (Fig. S7c).[11] Whereas, the peaks located at 162.3 and 161.2 eV can be assigned to S^{2-} $2p_{1/2}$ and S^{2-} $2p_{3/2}$ of sulfides for MnS, respectively (Fig. S7d).[11]

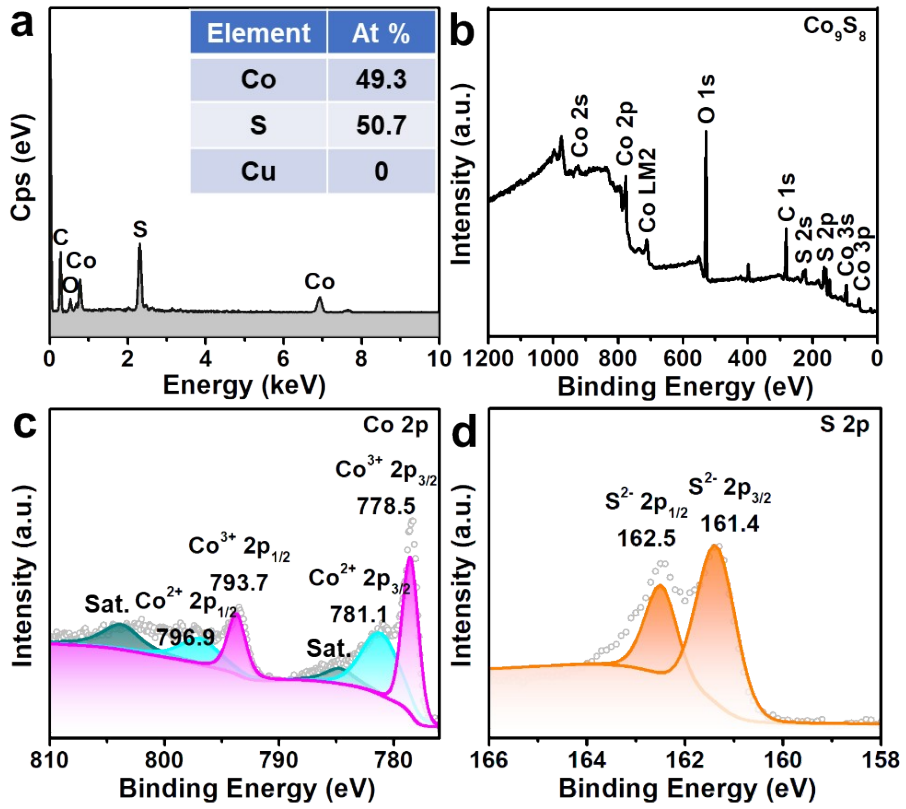

Fig. S8 (a) SEM-EDX profile and corresponding elemental contents (inset) of the synthesized Co_9S_8 icosapods. (b) Survey scan XPS spectrum and high-resolution XPS spectra of (c) Co 2p, and (d) S 2p for the Co_9S_8 icosapods, respectively.

The SEM-EDX profile shows that the atomic ratio of Co and S in the Co_9S_8 icosapods is ~0.97, which is close to the stoichiometric value of Co_9S_8, and there is no residual Cu element (Fig. S8a). The survey scan XPS spectrum discloses the presence of Co and S in the icosapods (Fig. S8b). For the Co 2p spectrum, the two peaks centering at 796.9 and 781.1 eV are characteristic to $2p_{1/2}$ and $2p_{3/2}$ of Co^{2+}, while the two peaks at 793.7 and 778.5 eV are assigned to $2p_{1/2}$ and $2p_{3/2}$ of Co^{3+}, respectively (Fig. S8c).[12,13] Furthermore, the fitted peaks at 803.8 and 784.7 eV belong to the shake-up satellite peaks of Co $2p_{3/2}$ and $2p_{1/2}$, respectively.[12,13] In Fig. S8d, two characteristic peaks in the S 2p spectrum are fitted at 162.5 and 161.4 eV, suggesting the typical $2p_{1/2}$ and $2p_{3/2}$of S^{2-} in Co_9S_8, respectively.[12,13]

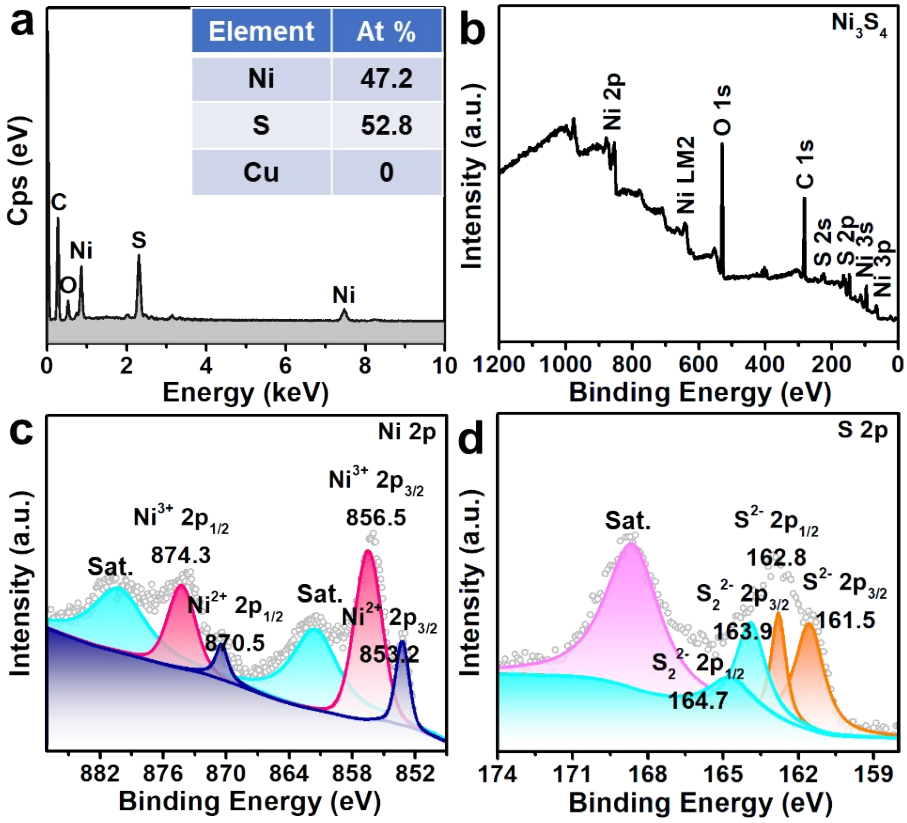

Fig. S9 (a) SEM-EDX profile and corresponding elemental contents (inset) of the synthesized Ni_3S_4 icosapods. (b) Survey scan XPS spectrum and high-resolution XPS spectra of (c) Ni 2p, and (d) S 2p for the Ni_3S_4 icosapods, respectively.

The SEM-EDX profile shows that the atomic ratio of Ni and S in Ni_3S_4 icosapods is ~0.89, which is close to the stoichiometric value of Ni_3S_4 and there is no residual Cu element (Fig. S9a). Fig. S9b also confirms the existence of Ni and S in the Ni_3S_4 icosapods. In the Ni 2p spectrum, the strong peaks located at 874.3 and 856.5 eV are assigned to Ni^{3+} $2p_{1/2}$ and Ni^{3+} $2p_{3/2}$ of Ni_3S_4, while the weak peaks at around 870.5 and 853.2 eV can be ascribed to Ni^{2+} $2p_{1/2}$ and Ni^{2+} $2p_{3/2}$ of sulfides for Ni_3S_4, respectively (Fig. S9c).[14,15] In addition, two broad peaks at 880.2 and 861.5 eV belong to satellite vibrational peaks of Ni $2p_{3/2}$ and $2p_{1/2}$, respectively.[14,15] For the S 2p spectrum, the peaks located at 164.7 and 163.9 eV can be ascribed to S_2^{2-} $2p_{1/2}$ and S_2^{2-} $2p_{3/2}$ of Ni_3S_4, whereas the peaks located at 162.8 and 161.5 eV can be assigned to S^{2-} $2p_{1/2}$ and S^{2-} $2p_{3/2}$ of sulfides for Ni_3S_4, respectively (Fig. S9d).[14,15.] A broad band located at 168.6 eV can be assigned to a vibrating satellite peak of S 2p.[14,15]

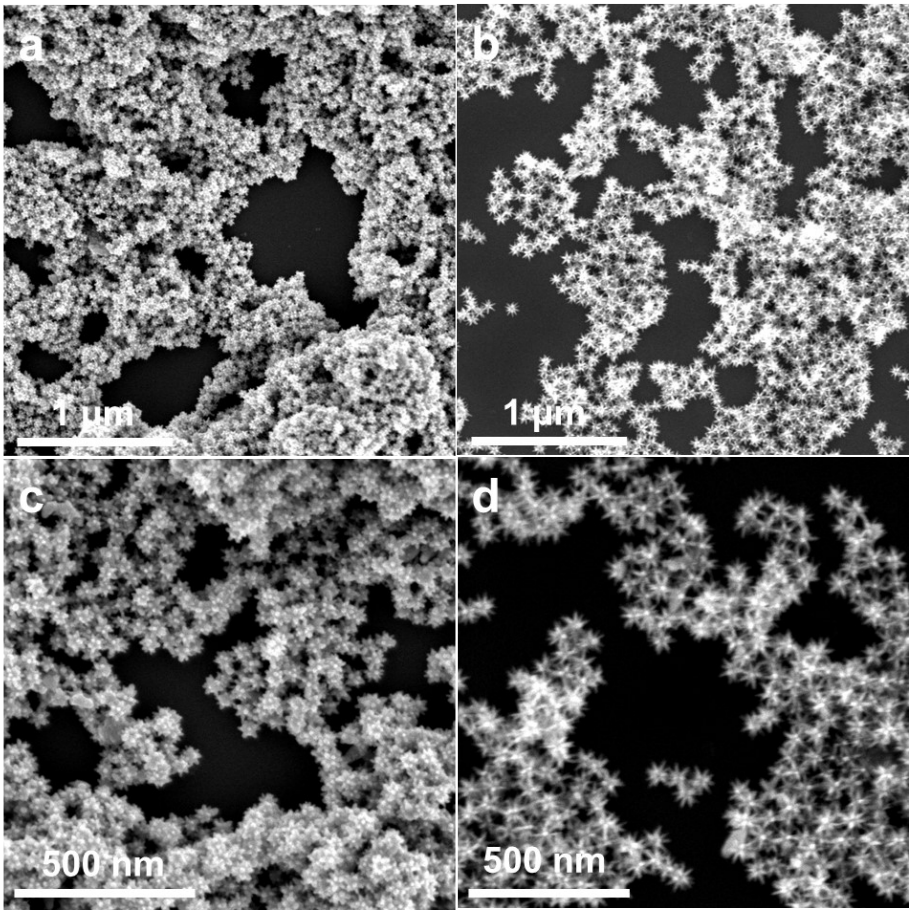

Fig. S10 SEM images of the (a, c) Pd_xS and (b, c) CdS-Pd_xS icosapods under different magnifications.

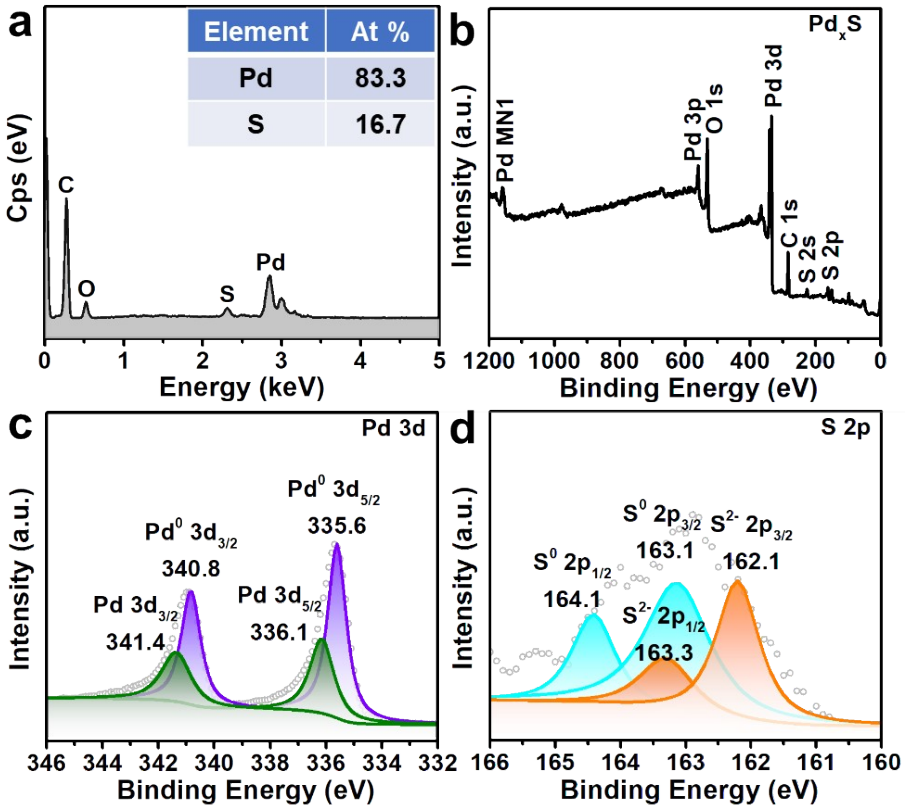

Fig. S11 (a) SEM-EDX profile and corresponding elemental contents (inset) of the synthesized Pd_xS icosapods. (b) Survey scan XPS spectrum and high-resolution XPS spectra of (c) Pd 3d, and (d) S 2p for the Pd_xS icosapods, respectively.

Fig. S11b verifies the presence of Pd and S in the Pd_xS icosapods. As for the Pd_xS icosapods, the signal for Pd 3d indicate the presence of two types of valence state (Fig. S11c). The strong peaks located at 340.8 and 335.6 eV can be ascribed to Pd^0 $2p_{3/2}$ and Pd^0 $2p_{5/2}$, while the weak peaks located at 341.4 and 336.1 eV can be assigned to Pd^{2+} $2p_{3/2}$ and Pd^{2+} $2p_{5/2}$, respectively.[7,16,17] There are also existed two types of valence state in the 2p S spectrum (Fig. S11d). The peaks located at 164.1 and 163.1 eV can be ascribed to S^0 $2p_{1/2}$ and S^0 $2p_{3/2}$, whereas the peaks located at 163.3 and 162.1 eV can be assigned to S^{2-} $2p_{1/2}$ and S^{2-} $2p_{3/2}$, respectively.[7,16,17] The ratio between the Pd^0 and the Pd^{2+} peaks was closer to 1.6:1, which is smaller than 3:1 as expected from the stoichiometry of the palladium sulfide.[7,16,17] The observed a larger ratio of Pd^{2+} was ascribing to the sulfur-enriched surfaces of Pd_xS according to the previous reports.[7,17]

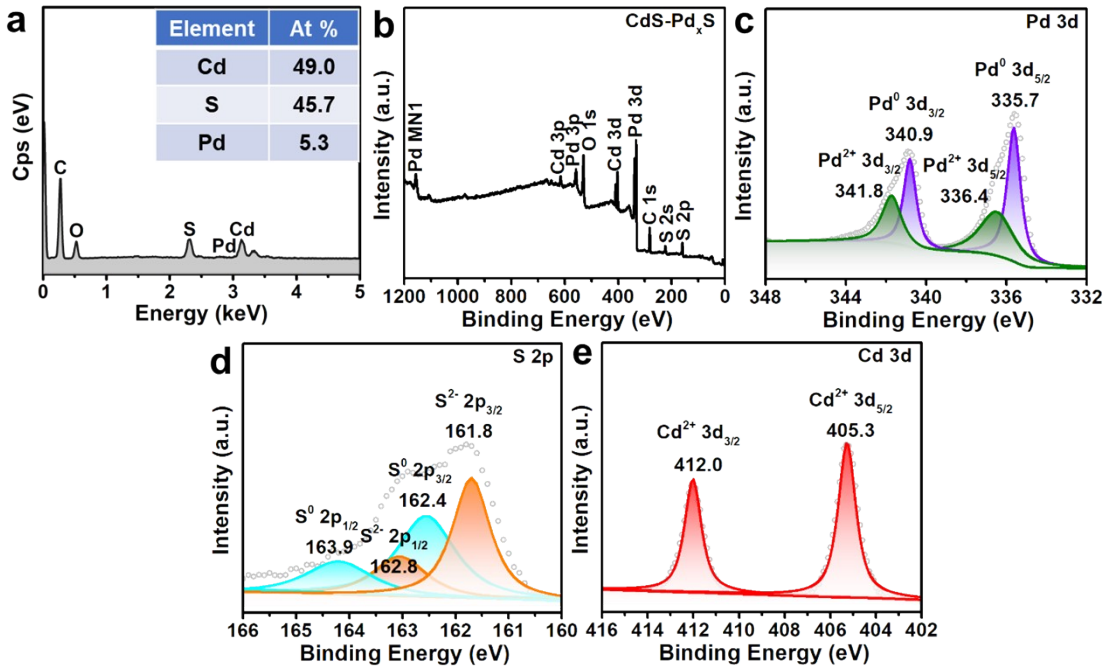

Fig. S12 (a) SEM-EDX profile and the corresponding elemental contents (inset) of the CdS-Pd$_x$S icosapods. (b) Survey scan XPS spectrum and high-resolution XPS spectra of (c) Pd 3d, (d) S 2p, and (e) Cd 2d for the CdS-Pd$_x$S icosapods.

As seen in Fig. S12b, survey scan XPS spectrum confirms the existence of Cd, Pd and S in the CdS-Pd$_x$S icosapods. The Pd 3d and S 2p spectra for CdS-Pd$_x$S icosapods were similar to Pd$_x$S icosapods (Fig. S12c and d). The spectrum of Cd 3d shows two binding energies at 412.0 and 405.3 eV, which can be ascribed to Cd^{2+} $3d_{3/2}$ and Cd^{2+} $3d_{5/2}$ of CdS-Pd$_x$S icosapods, respectively (Fig. S12e).[8]

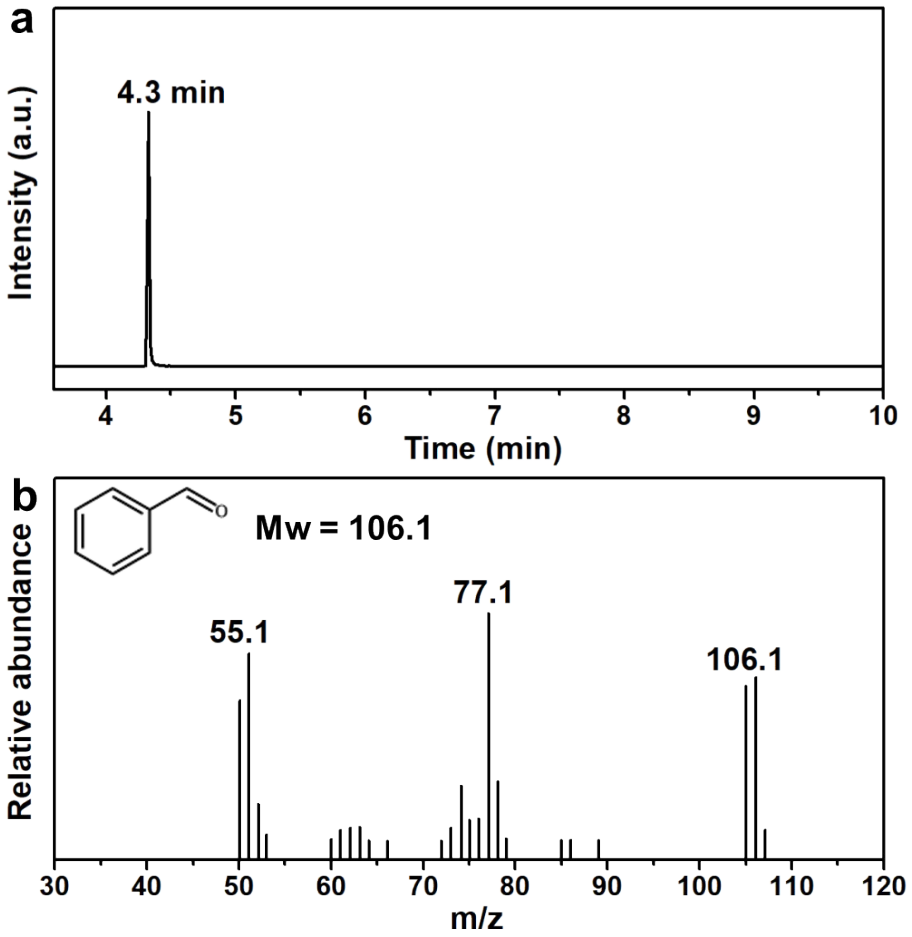

Fig. S13 (a) GC-MS and (b) mass spectra for the obtain liquid-products of BA photoreformed by the CdS-Pd_xS icosapods.

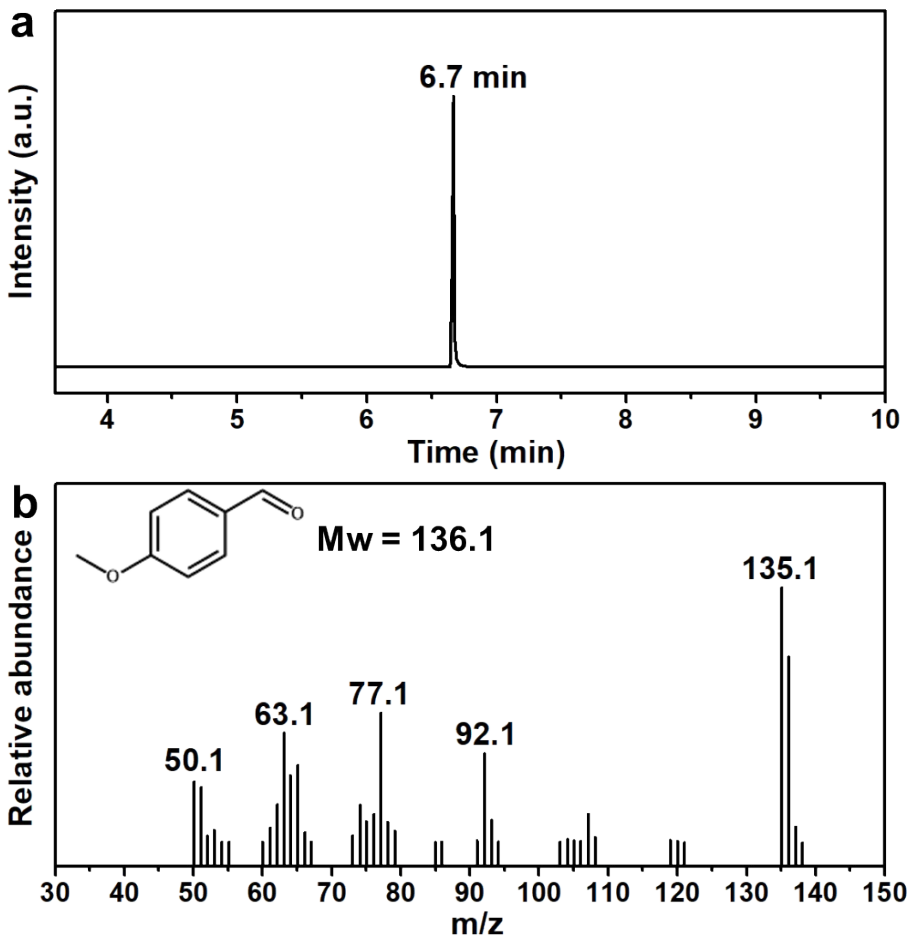

Fig. S14 (a) GC-MS and (b) mass spectra for the obtain liquid-products of 4-OCH_3-BA photoreformed by the CdS-Pd_xS icosapods.

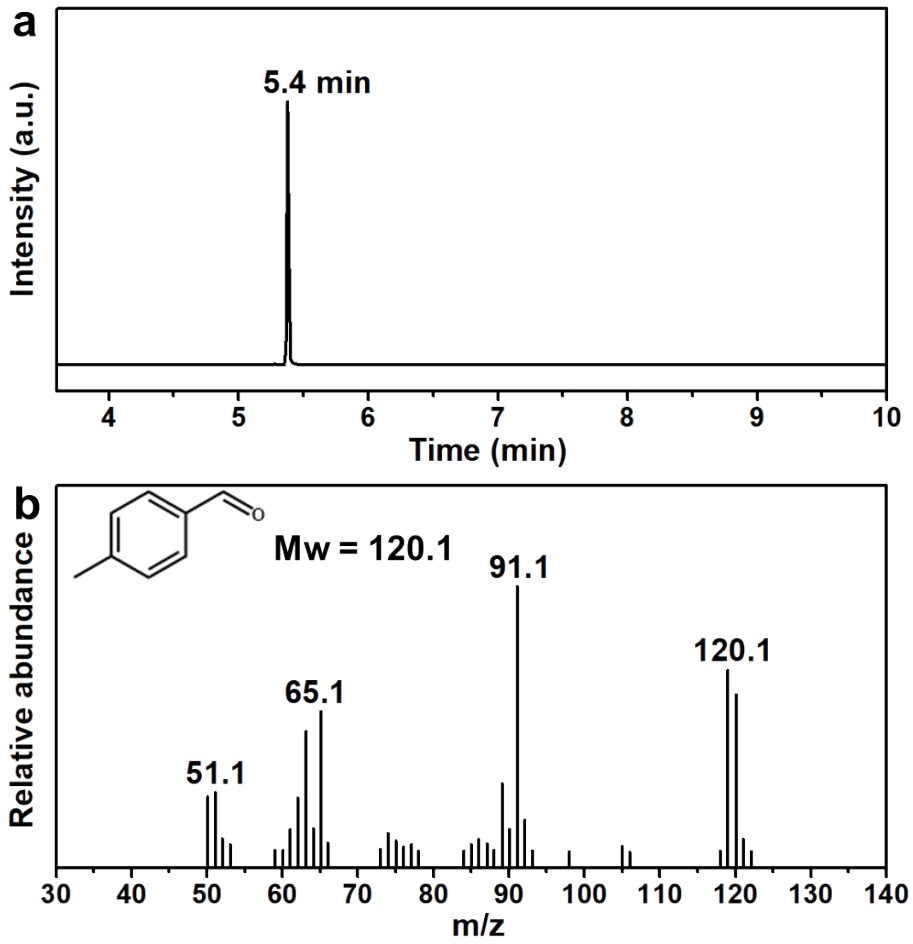

Fig. S15 (a) GC-MS and (b) mass spectra for the obtain liquid-products of 4-CH_3-BA photoreformed by the CdS-Pd_xS icosapods.

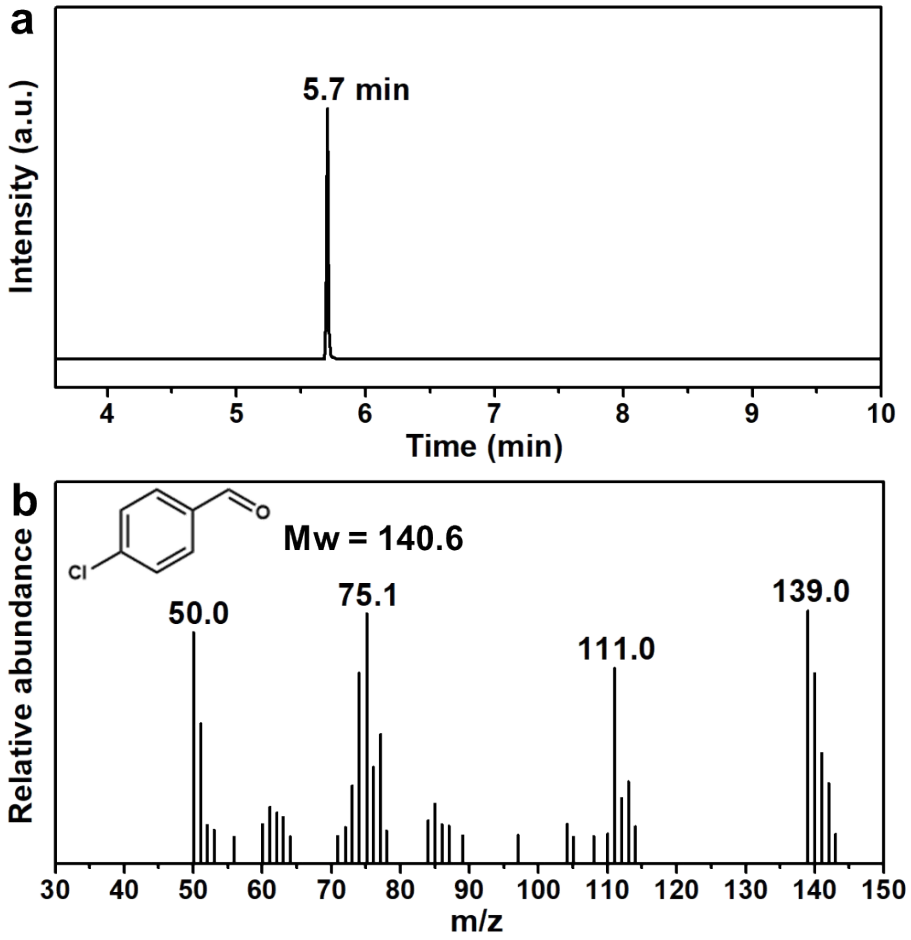

Fig. S16 (a) GC-MS and (b) mass spectra for the obtain liquid-products of 4-Cl-BA photoreformed by the CdS-Pd_xS icosapods.

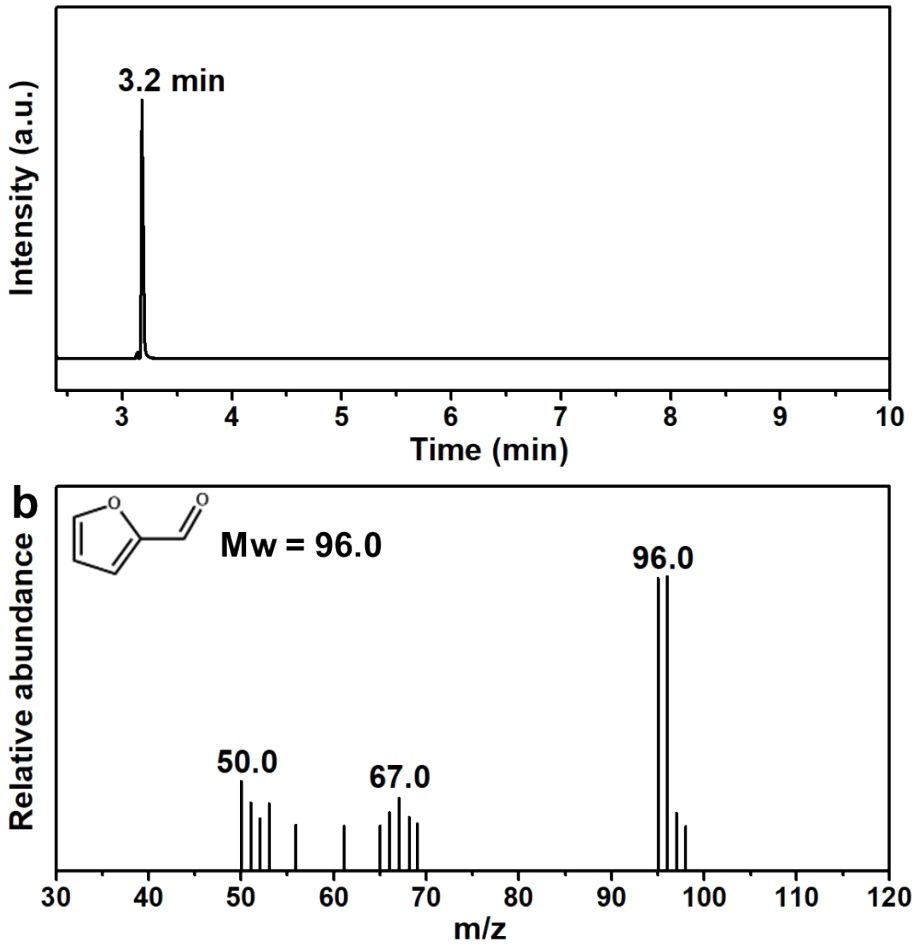

Fig. S17 (a) GC-MS and (b) mass spectra for the obtain liquid-products of FA photoreformed by the CdS-Pd_xS icosapods.

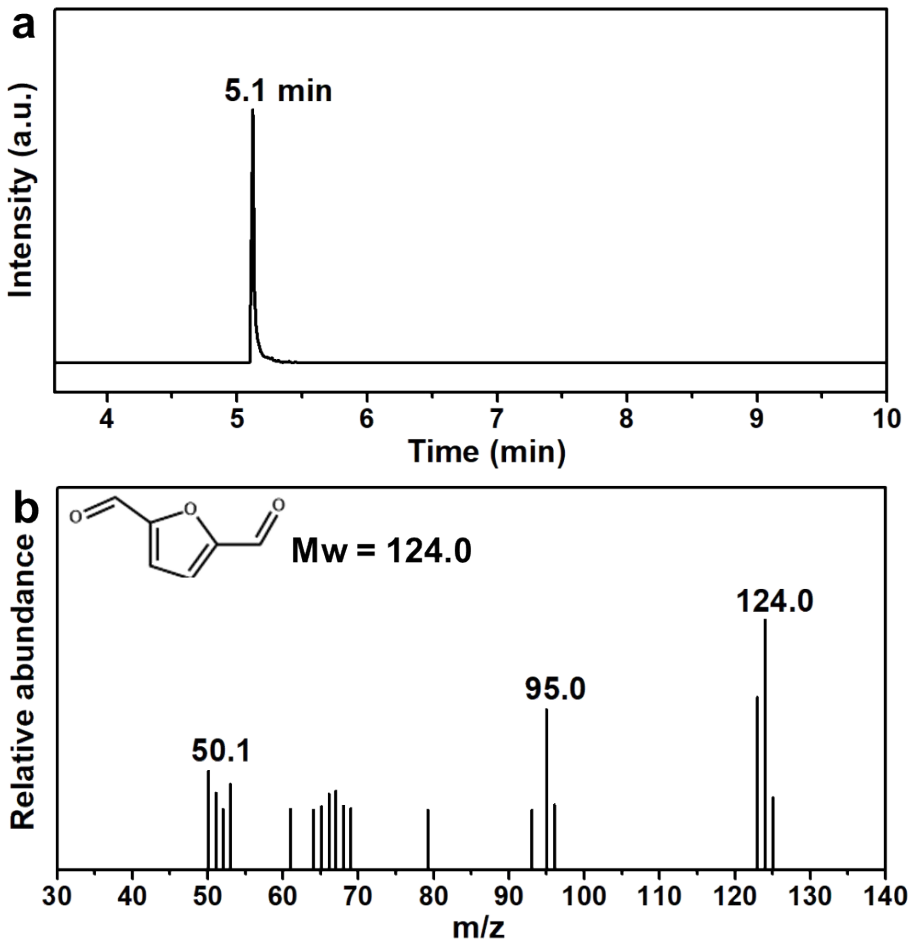

Fig. S18 (a) GC-MS and (b) mass spectra for the obtain liquid-products of HMF photoreformed by the CdS-Pd_xS icosapods.

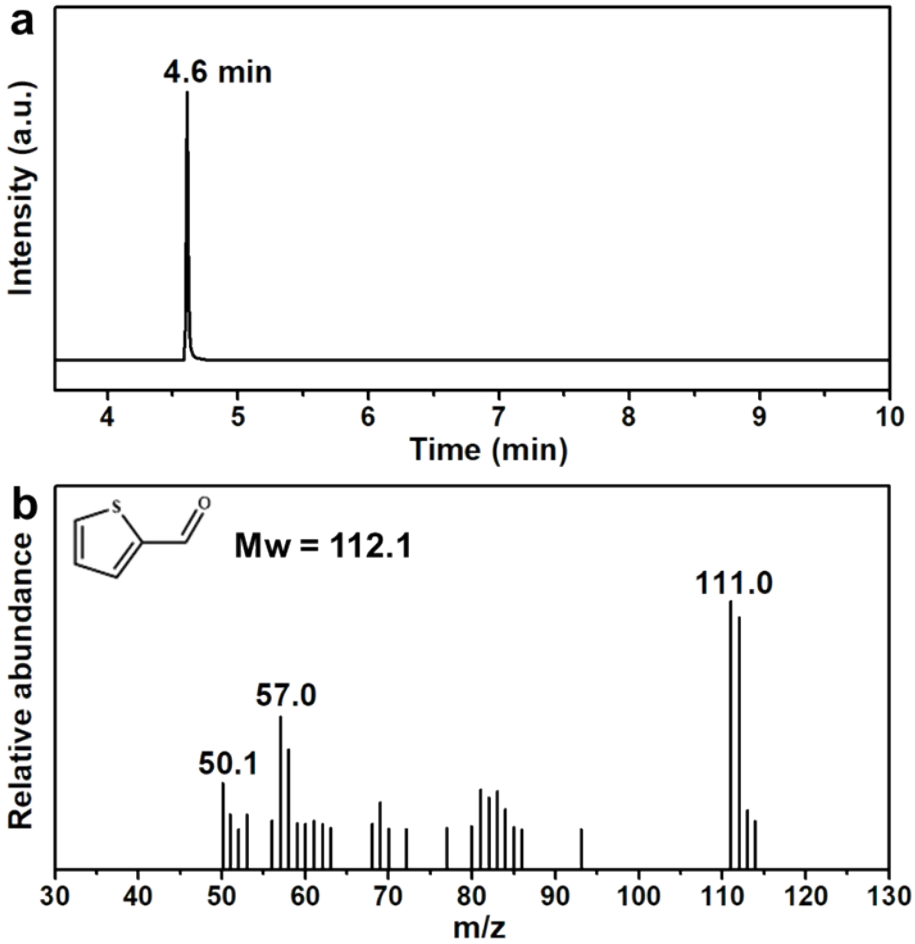

Fig. S19 (a) GC-MS and (b) mass spectra for the obtain liquid-products of 2-thiophenemethanol photoreformed by the CdS-Pd_xS icosapods.

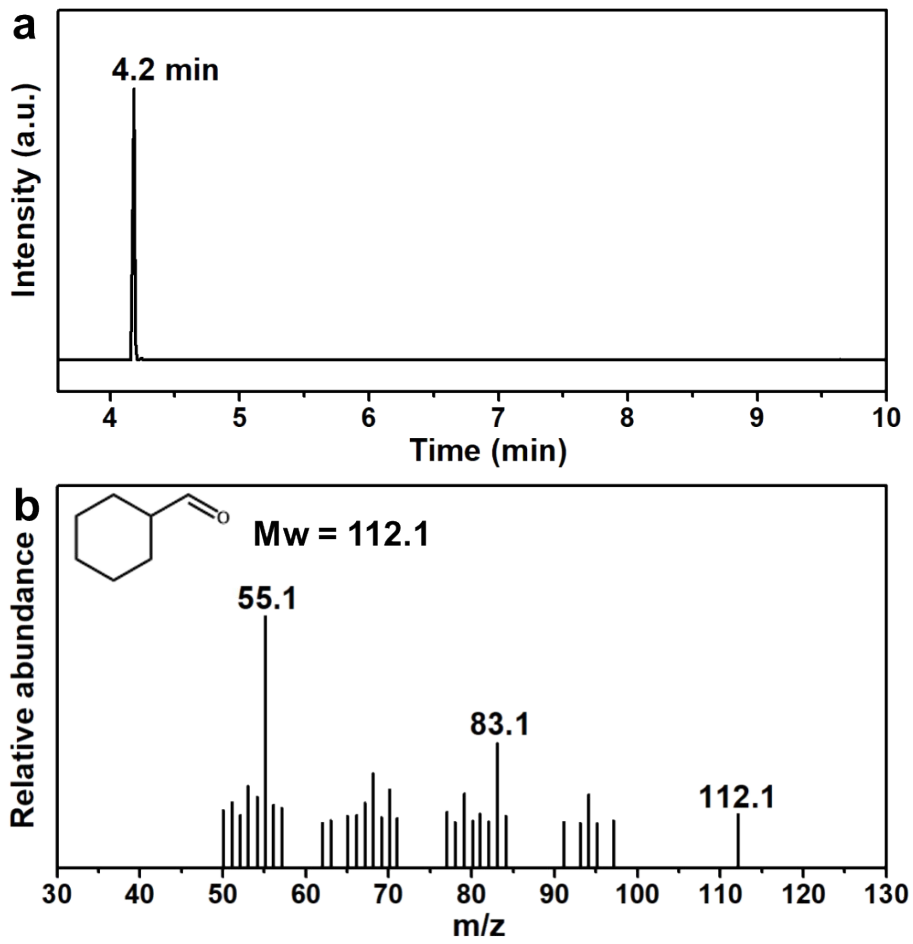

Fig. S20 (a) GC-MS and (b) mass spectra for the obtain liquid-products of cyclohexanemethanol photoreformed by the CdS-Pd_xS icosapods.

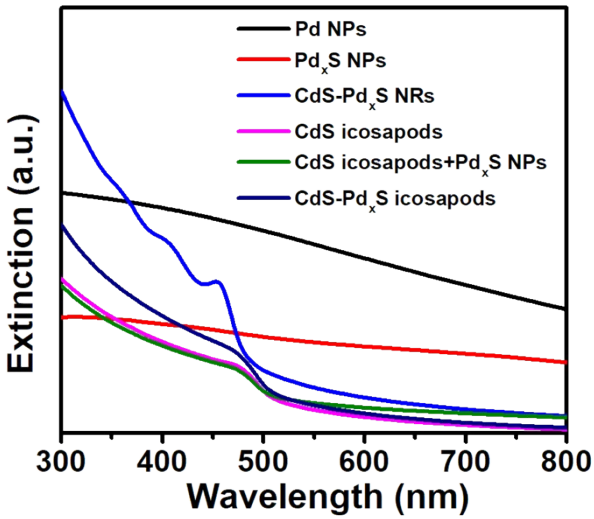

Fig. S21 The UV-vis extinction spectra of Pd NPs, Pd_xS NPs, CdS-Pd_xS NRs, CdS icosapods, physical mixture of CdS icosapods and Pd_xS NPs, and CdS-PdxS icosapods.

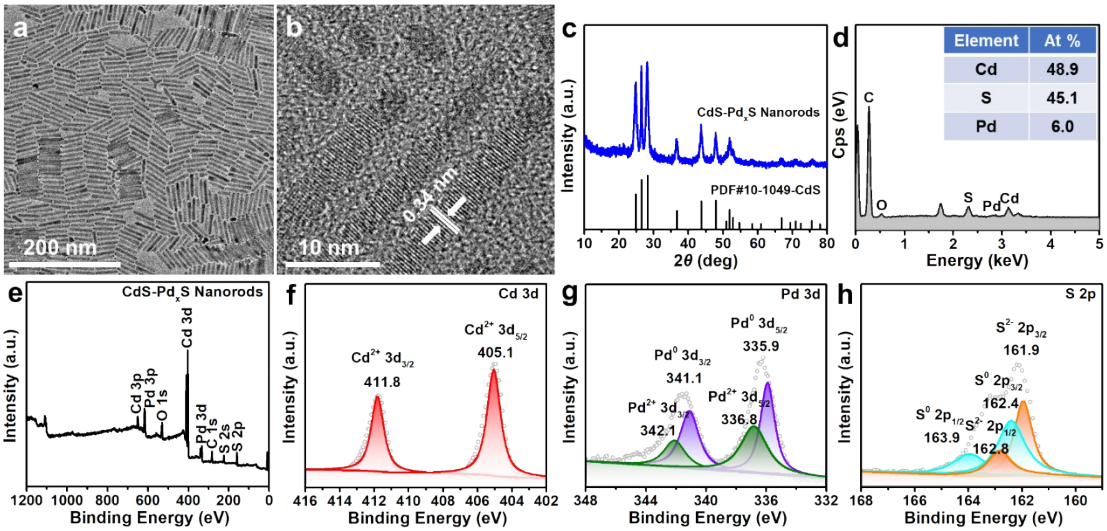

Fig. S22 (a) TEM, (b) HRTEM, and (c) XRD pattern of the CdS-Pd$_x$S NRs. (d) SEM-EDX profile and the corresponding elemental contents (inset) of the CdS-Pd$_x$S NRs. (e) Survey scan XPS spectrum and high-resolution XPS spectra of (f) Cd 3d, (g), Pd 3d, and (h) S 2p for the CdS-Pd$_x$S NRs, respectively.

The TEM image reveal that both of the tip areas of CdS NRs have been cation exchanged by Pd^{2+}, producing the CdS-Pd$_x$S NRs (Fig. S22a). HRTEM image of CdS-Pd$_x$S NRs discloses the disorder arrangement for the Pd$_x$S tips, while the CdS backbones show clear lattice fringes (Fig. S22b). As seen in Fig. S22c, the XRD pattern of the obtained CdS-Pd$_x$S NRs was matched well with the wurtzite structure of CdS. The SEM-EDS profile shows that the atomic ratio of Pd in CdS-Pd$_x$S NRs is 6.0% (Fig. S22d). The Cd, Pd, and S are existed in the CdS-Pd$_x$S NRs by XPS survey scans (Fig. S22e). The peaks located at 411.8 and 405.1 eV can be ascribed to Cd^{2+} $3d_{3/2}$ and Cd^{2+} $3d_{5/2}$ of CdS, respectively (Fig. S22f).[7] The peaks presented for Pd 3d indicate the presence of two valence states of Pd. The strong peaks located at 341.1 and 335.9 eV can be ascribed to Pd^0 $2p_{3/2}$ and Pd^0 $2p_{5/2}$ of metallic Pd, while the peaks located at 342.1 and 336.8 eV can be assigned to Pd^{2+} $2p_{3/2}$ and Pd^{2+} $2p_{5/2}$ of CdS-Pd$_x$S NRs, respectively (Fig. S22g).[7] There are also existed two types of valence state in the S 2p spectrum (Fig. S22h). The peaks located at 163.9 and 162.4 eV can be ascribed to S^0 $2p_{1/2}$ and S^0 $2p_{3/2}$ of CdS-Pd$_x$S NRs, whereas the peaks located at 162.8 and 161.9 eV can be assigned to S^{2-} $2p_{1/2}$ and S^{2-} $2p_{3/2}$ of CdS-Pd$_x$S NRs, respectively.[7]

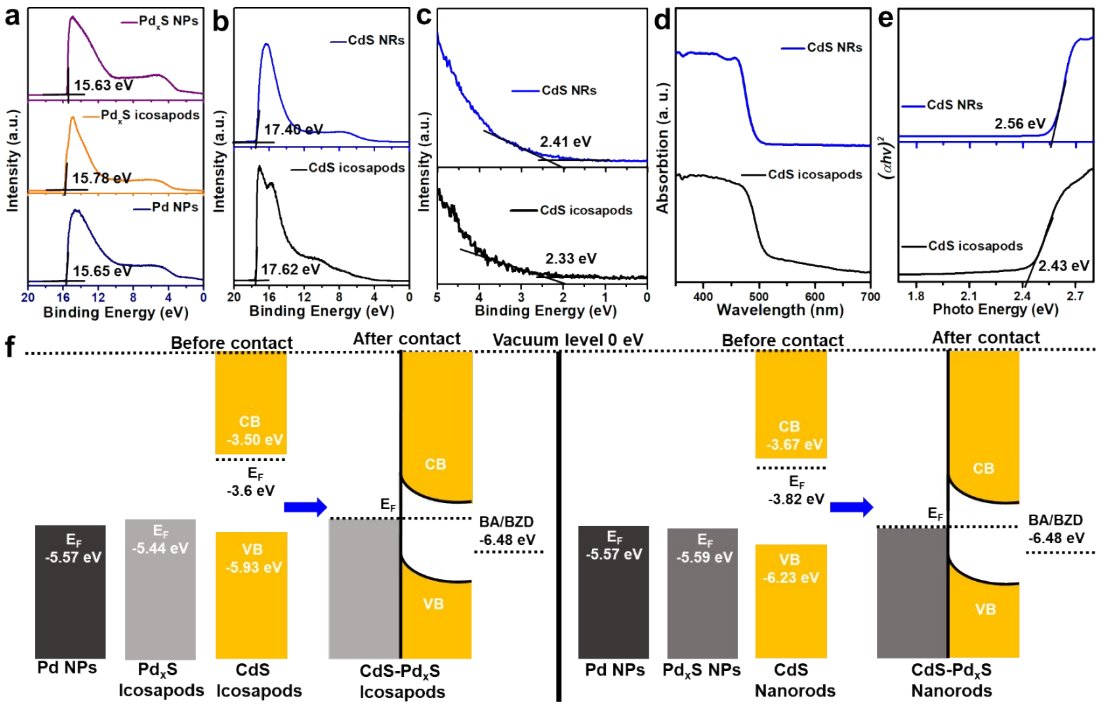

Fig. S23 (a-b) The UPS spectra of Pd NPs, Pd_xS icosapods, Pd_xS NPs, CdS icosapods, and CdS NRs, respectively. (c) Magnified view of the low binding energy region of UPS spectra for CdS icosapods and CdS NRs. (d) UV−vis DRS and (e) Corresponding plots of $(\alpha hv)^2$ versus photoenergy (hv) for CdS icosapods and CdS NRs. (f) Bandgap structures of CdS-Pd_xS icosapods (left panel) and nanorods (right panel).

To reveal the interfacial electronic structure of the CdS-Pd_xS icosapods and nanorods, the ultraviolet photoelectron spectroscopy (UPS) has been used to determine valence and conduction bands of these nanostructures. The corresponding work functions (Φ) can be estimated according to the following equation: $\Phi = hv - |E_{cut\text{-}off} - E_f|$, where hv was the fixed incident photon energy of 21.22 eV (He I lamp) and E_f was calibrated to 0 eV using a standard Au sample. As shown in Fig. S23a-b, the cut-off energies ($E_{cut\text{-}off}$) of Pd NPs, Pd_xS icosapods, Pd_xS NPs, CdS icosapods, and CdS NRs are determined to be 15.65, 15.78, 15.63, 17.62, and 17.40 eV respectively. The Φ of the different samples are estimated to be 5.57, 5.44, 5.59, 3.60, and 3.82 eV, respectively. So, the Femi level (E_F) of the different samples are estimated to be −5.57, −5.44, −5.59, −3.60, and −3.82 eV (*vs.* Vacuum), respectively. The difference between E_F and valence band maximum (E_V) is determined by the intersection of the linear portion of the spectra near the Fermi

edge (low binding energy region) with the baseline (Fig. S23c). Therefore, the E_V of CdS icosapods and NRs are −5.93 and −6.23 eV (*vs.* Vacuum), respectively. The conduction band minimum (E_C) is further calculated by E_V adding the optical bandgap (Fig. S23d-e, 2.43 eV for CdS icosapods and 2.56 eV for CdS nanorods). Here, the E_C of CdS icosapods and nanorods should be −3.50 and −3.67 eV (*vs.* Vacuum), respectively. In all, the corresponding bandgap structures of CdS-Pd_xS icosapods and nanorods as well as the oxidation potential of BA/BAD are depicted in the Fig. S23f. An apparent Schottky junction was formed in both CdS-Pd_xS samples due to very closed Fermi level of Pd NPs with respect to Pd_xS. In addition, the as-prepared CdS-Pd_xS icosapods and nanorods photocatalysts not only meet the reduction potential required for the conversion of H^+ to H_2, but also meet the oxidation potential of selective oxidation of BA to BAD. In all, the electronic structures of both CdS-Pd_xS icosapods and CdS-Pd_xS NRs are quite similar.

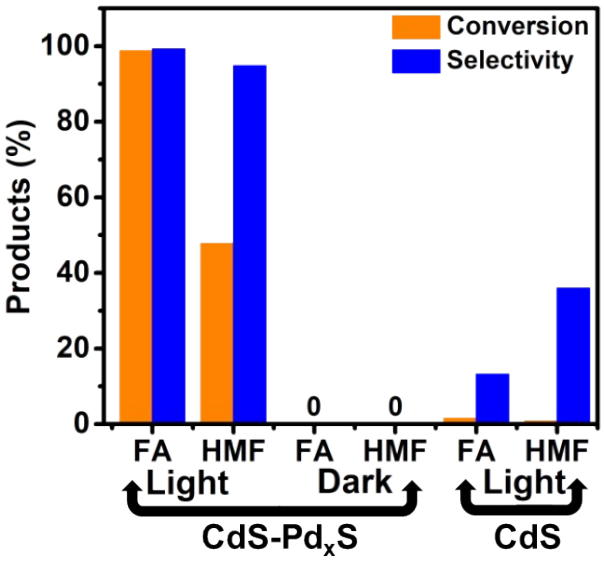

Fig. S24 The photocatalytic performance of HMF and FA over CdS-Pd_xS and CdS icosapods under light and dark conditions.

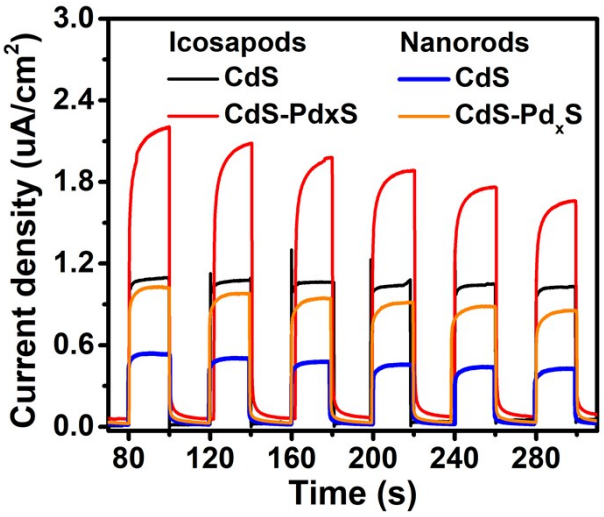

Fig. S25 Transient photocurrent responses for the CdS and CdS-Pd_xS icosapods, CdS and CdS-Pd_xS nanorods.

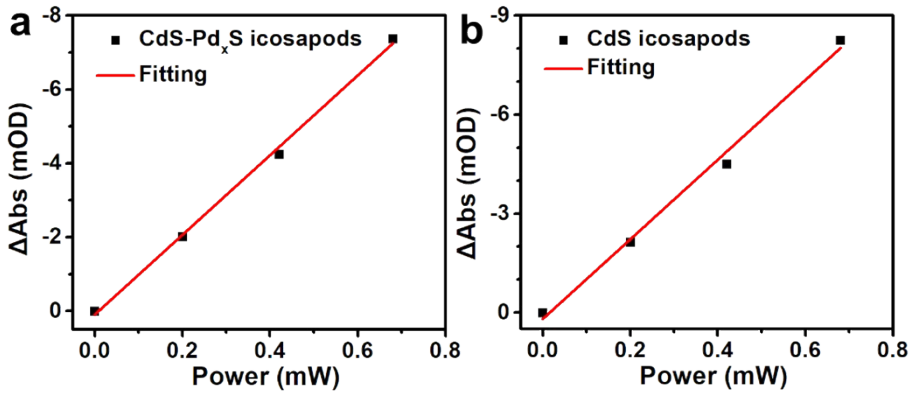

Fig. S26 The power-dependence absorption plots of the (a) CdS-Pd_xS and (b) CdS icosapods.

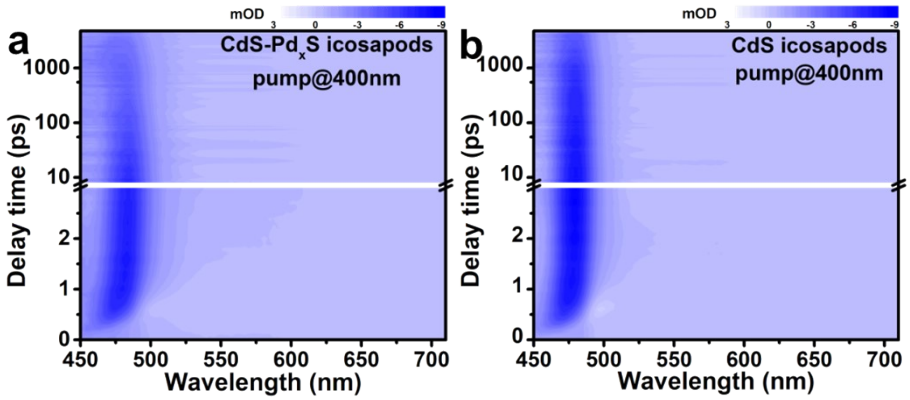

Fig. S27 Two-dimensional pseudo-color plots of TA spectra for the (a) CdS-Pd_xS and (b) CdS icosapods in toluene pumped by 400 nm laser.

Table S1 Summary of some previous representative works on photoreforming biomass-relevant alcohols coupled with H_2 evolution under different conditions.

Catalyst	Light source	Reaction conditions	Liquid products	H_2 product mmol/g/h	Ref
CdS-Pd_xS	**300 W Xe-lamp λ > 420 nm**	**N_2, 10 mg catalyst 10 mM aromatic alcohols 2–2.5h, 10 mL CH_3CN**	**Aromatic aldehydes Sel. > 99 % Con. > 97 %**	**16.01 AQY: 31.4 % (420nm, BA)**	**This work**
CdS-Pd_xS	**300 W Xe-lamp λ > 420 nm**	**N_2, 10 mg catalyst 10 mM FA (HMF) 4 h (8 h), 10 mL CH_3CN**	**FF (DFF) Sel. 99 (95) % Con. 98 (48) %**	**2.41 (0.54)**	**This work**
$Zn_3In_2S_6$	300 W Xe-lamp λ > 380 nm	Vacuum, 100 mg catalyst 4 h, 100 mL BA	BZD	1.80	S18
$Au/ZnIn_2S_4$	300 W Xe-lamp λ ≥ 420 nm	Vacuum, 50 mg catalyst 4 h, 5 mL BA+45 mL H_2O	BZD	1.63	S19
Pd/ $CdS-TiO_2$	LED lamp λ_{max} = 460 nm,	Ar, 50 mg catalyst 0.05 mmol BA 4 h, 10 mL H_2O	BZD Sel. 99 % Con. 96 %	1.20 AQY: 3.5 % (480 nm)	S20
Ni/CdS	7 W blue LED	Ar, 6 mg catalyst 0.2 mmol BA 20 h, 3 mL CH_3CN	BZD Sel. 96 % Con. 96 %	_	S21
Co-CdS	300 W Xe-lamp λ > 420 nm	Ar, 5 mg catalyst 3 h, 20 mL BA	BZD Sel. 94 %	13.47 AQY: 63.2 % (420 nm)	S22
$Pt/Zn_3In_2S_6$	300 W Xe-lamp λ ≥ 420 nm	Ar, 180 mg catalyst 0.2 M BA 12 h, 50 mL BTF	BZD Sel. 93 %	0.91 AQY: 4.6 % (400 nm)	S23
Ni/ $Zn_{0.5}Cd_{0.5}S$	300 W Xe-lamp λ > 420 nm	Ar, 5 mg catalyst 3 h, 20 mL BA	BZD Sel. 58 % Con. 40 %	18.9 AQY: 52.5 % (420 nm)	S24
Au-Pt@CdS	300 W Xe-lamp λ ≥ 420 nm	Ar, 2 mg catalyst 1 mmol BA 5 h, 2 mL BTF	BZD Sel. 94 % Con. 80 %	76.5 AQY: ~31 % (400 nm)	S25
MPA-CdSe QDs-Ni^{2+}	Purple LED 410 nm	Ar 0.1 mmol BA 6 h, 5 mL H_2O	BZD Sel. 98 % Con. 92 %	_	S26
$ZnS-Ni_xS_y$	500 W Xe lamp 200 nm	N_2, 20 mg catalyst 5 mM BA 3 h, 100 mL H_2O	BZD Sel. 91 % Con. 42 %	3.65	S27

Co_9S_8/CdS	LED lamp 450 nm	Ar, 1 mg catalyst 96 mM BA 6 h, 5 mL H_2O	BZD Sel. 100 % Con. 72 %	4.32	S28
CdS QDs-NiAl-LDL	White LED 50 W × 4 λ > 400 nm	Ar, 1 mg catalyst 20 mM 4-OCH_3-BA 3 h, 10 mL H_2O	4-OCH_3-BZD Sel. 99 % Con. 99 %	73.23 AQY: 16.5 % (420 nm)	S29
Au_2S@CdS	6 W blue LED 445 nm	Ar, 5 mg catalyst 0.1 M BA 4 h, 1 mL CH_3CN	BZD Sel. 99 % Con. 99 %	_	S30
$ZnIn_2S_4$/Nix-B	300 W Xe-lamp λ > 400 nm	Ar, 10 mg catalyst 0.2 mmol BA 2 h, 3 mL CH_3CN	BZD Sel. 96 %	8.90 AQY: 24.0 % (420 nm)	S31
Ni/CdS	8 W blue LED 440–460nm	N_2, 10 mg catalyst 10 mM HMF (FA) 24 h, 10 mL H_2O	DFF (FF) Sel. 100 (100) % Con. 24 (100) %	_	S32
$Zn_{0.5}Cd_{0.5}S$-P	30 × 3 W White LED	Ar, 1 mg catalyst 2 mg/mL HMF 8 h, 5 mL H_2O	DFF Sel. 65 % Con. 40 %	0.79	S33
NiS/$Zn_3In_2S_6$	300 W Xe-lampλ > 400 nm	Vacuum, 0.1 g catalyst 0.1 M HMF 4 h, 50 mL H_2O	DFF Sel. 94.1 %	0.12 AQY: 1.35 % (400 nm)	S34
$Zn_{0.5}Cd_{0.5}S$/MnO_2	30 W white LED λ ≥ 400 nm	N_2, 20 mg catalyst 2 mg/mL HMF 24 h, 10 mL H_2O	DFF Sel. 100 % Con. 47 %	0.06	S35
CoP/$Zn_{0.5}Cd_{0.5}S$	300 W Xe-lamp, λ > 420 nm	Vacuum, 100 mg catalyst 0.1 M HMF 4 h, 50 mL H_2O	DFF Sel. 87 % Con. 33 %	0.60 AQY: 4.1 % (400 nm)	S36
RuTBC-CdS QDs	300 W Xe-lampλ > 300 nm	Ar, 10 mg catalyst 0.1 mmol HMF (FA) 20 h, 10 mL DMF	DFF (FF) Sel. > 92 % Con. > 81 (15.2) %	_	S37
$Ti_3C_2T_x$/CdS	300 W Xe-lamp λ > 420 nm	N_2, 10 mg catalyst 25 μmol FA 10 h, 10 mL H_2O	FF Sel. 93 % Con. ~100 %	0.19	S38
MoS_2-$ZnIn_2S_4$	300 W Xe-lamp λ > 420 nm	Ar, 5 mg catalyst 0.1 mmol FA 5 h, 10 mL H_2O	FF Sel. 95 %	2.75 AQY: ~3 % (400 nm)	S39
$ZnIn_2S_4$/Tp-Tta	80 W LED λ = 420 nm	N_2, 10 mg catalyst 8 mL FA 3 h, 72 mL H_2O	FF	9.73 AQY: 6.2% (420 nm)	S40

Note: BA, BZD, HMF, DFF, FA, FF, BTF, 4-OCH_3-BA, 4-OCH_3-BAD and DMF refers to benzyl alcohol, benzaldehyde, 5-hydroxymethylfurfural, 2, 5-diformylfurane, furfuryl alcohol, furfural, benzotrifluoride, 4-methoxybenzyl alcohol, 4-

methoxybenzaldehyde and *N, N*-Dimethylformamide, respectively. Sel. and Con. refers to selectivity and conversion, respectively. AQY refers to apparent quantum yield.

References

1 S. Peng, J. M. McMahon, G. C. Schatz, S. K. Gray, Y. Sun, *Proc. Natl. Acad. Sci. U. S. A.* **2010**, *107*, 14530–14534.

2 L. Zhai, S. T. Gebre, B. Chen, D. Xu, J. Chen, Z. Li, Y. Liu, H. Yang, C. Ling, Y. Ge, W. Zhai, C. Chen, L. Ma, Q. Zhang, X. Li, Y. Yan, X. Huang, L. Li, Z. Guan, C.-L. Tao, Z. Huang, H. Wang, J. Liang, Y. Zhu, C.-S. Lee, P. Wang, C. Zhang, L. Gu, Y. Du, T. Lian, H. Zhang, X.-J. Wu, *Nature Commun.,* **2023**, *14*, 2538–2547.

3 H. Li, M. Zanella, A. Genovese, M. Povia, A. Falqui, C. Giannini, L. Manna, *Nano Lett*. **2011**, *11*, 4964–4970.

4 A. E. Powell, J. M. Hodges, R. E. Schaak, *J. Am. Chem. Soc.* **2016**, *138*, 471–474.

5 A. G. Butterfield, C. R. McCormick, J. M. Veglak, R. E. Schaak, *J. Am. Chem. Soc.* **2021**, *143*, 7915–7919.

6 Z. Li, M. Saruyama, T. Asaka, Y. Tatetsu, T. Teranishi, *Science* **2021**, *373*, 332–337.

7 Y. Shemesh, J. E. Macdonald, G. Menagen, U. Banin, *Angew. Chem. Int. Ed.* **2011**, *50*, 1185–1221.

8 C. O'Sullivan, R. D. Gunning, A. Sanyal, C. A. Barrett, H. Geaney, F. R. Laffir, S. Ahmed, K. M. Ryan, *J. Am. Chem. Soc.* **2009**, *131*, 12250–225.

9 H. Jiang, H. Peng, H. Guo, Y. Zeng, L. Li, Y. Zhang, Y. Chen, X. Chen, J. Zhang, R. Chu, *ACS Appl. Mater. Interfaces* **2020**, *12*, 46, 51344–51356.

10 S. Kumar, S. Riyajuddin, M. Afshan, S. T. Aziz, T. Maruyama, K Ghosh, *J. Phys. Chem. Lett.* **2021**, *12*, 6574–6581.

11 P. Tiwari, G. Malik, R. Chandra, *J. Appl. Phys*. **2018**, *124*, 195106–195118.

12 X. Yuan, J. Yin, Z. Liu, X. Wang, C. Dong, W. Dong, M. S. Riaz, Z. Zhang, M.-Y. Chen, F. Huang, *ACS Appl. Mater. Interfaces* **2018**, *10*, 11565−11571.

13 M. Yin, X. Feng, D. Zhao, Y. Zhao, H. Li, W. Zhou, H. Liu, X. Bai, H. Wang, C. Feng, Q. Jiao, *ACS Sustainable Chem. Eng.* **2019**, *7*, 6122–6130.

14 J.-T. Ren, Z.-Y. Yuan, *ACS Sustainable Chem. Eng.* **2017**, *5*, 7203–7210.

15 J.-Y. Wu, T.-H. Lai, M.-J. Fang, J.-Y. Chen, M.-Y. Kuo, Y.-H. Chiu, P.-Y. Hsieh, C.-W. Tsao, H.-E. Chang, Y.-P. Chang, C.-Y. Wang, C.-Y. Chen, M. Sone, W.-W. Wu, T.-F. M. Chang, Y.-J. Hsu, *ACS Appl. Nano Mater.* **2022**, *5*, 8404−8416.

16 L. L. Long, A. Y. Zhang, Y. X. Huang, X. Zhang, H. Q. Yu, *J. Mater. Chem. A* 2**015**, *3*, 4301–4306.

17 C. Du, P. Li, F. Yang, G. Cheng, S. Chen, W. Luo, *ACS Appl. Mater. Interfaces* **2018**, *10*, 753–761.

18 X. Ye, Y. Chen, Y. Wu, X. Zhang, X. Wang, S. Chen, *Appl. Catal., B* **2019**, *242*, 302–311.

19 T. Zhu, X. Ye, Q. Zhang, Z. Hui, X. Wang, S. Chen, *J. Hazard. Mater.* **2019**, *367*, 277–285.

20 S. Higashimoto, Y. Tanaka, R. Ishikawa, S. Hasegawa, M. Azuma, H. Ohue, Y. Sakata, *Catal. Sci. Technol*. **2013**, *3*, 400–403.

21 Z. Chai, T.-T. Zeng, Q. Li, L.-Q. Lu, W.-J. Xiao, D. Xu, *J. Am. Chem. Soc.* **2016**, *138*, 10128–1013

22 D. C. Jiang, X. Chen, Z. Zhang, L. Zhang, Y. Wang, Z. J. Sun, R. M. Irfan, P. W. Du, *J. Catal.* **2018**, *357*, 147–153.

23 S. Meng, X. Ye, J. Zhang, X. Fu, S. Chen, *J. Catal.* **2018**, *367*, 159–170.

24 L. Zhang, D. Jiang, R. M. Irfan, S. Tang, X. Chen, P. Du, *J. Energy Chem.* **2019**, *30*, 71–77.

25 C. Han, Z.-R. Tang, J. Liu, S. Jin, Y.-J. Xu, *Chem. Sci.* **2019**, *10*, 3514–3522.
26 L.-M. Zhao, Q.-Y. Meng, X.-B. Fan, C. Ye, X.-B. Li, B. Chen, V. Ramamurthy, C.-H. Tung, L.-Z. Wu, *Angew. Chem. Int. Ed.* **2017**, *56*, 3020–3024.
27 H. Hao, L. Zhang, W. Wang, S. Qiao, X. Liu, *ACS Sustainable Chem. Eng.* **2019**, *7*, 10501–10508.
28 M. Liu, L. Qiao, B. Dong, S. Guo, S. Yao, C. Li, Z. Zhang, T. Lu, *Appl. Catal., B* **2020**, *273*, 119066–119073.
29 L. Jiao, D. Zhang, Z. Hao, F. Yu, X.-J. Lv, *ACS Catal.* **2021**, *11*, 8727–8735.
30 S. G. Lee, M. J. Kang, M. Park, K.-J. Kim, H. Lee, H. S. Kim, *Appl. Catal. B: Environ.* **2022**, *304*, 120967–120978.
31 X. Li, S. Lu, J. Yi, L. Shen, Z. Chen, H. Xue, Q. Qian, M.-Q. Yang, *ACS Appl. Mater. Interfaces* **2022**, *14*, 25297–25307.
32 G. Han, Y.-H. Jin, R. A. Burgess, N. E. Dickenson, X.-M. Cao, Y. Sun, *J. Am. Chem. Soc.* **2017**, *139*, 15584–15587.
33 H.-F. Ye, R. Shi, X. Yang, W.-F. Fu, Y. Chen, *Appl. Catal., B* **2018**, *233*, 70–79.
34 S. Meng, H. Wu, Y. Cui, X. Zheng, H. Wang, S. Chen, Y. Wang, X. Fu, *Appl. Catal. B* 2020, *266*, 118617–118626.
35 S. Dhingra, T. Chhabra, V. Krishnan, C. M. Nagaraja, *ACS Appl. Energy Mater.* **2020**, *3*, 7138–7148.
36 Y. Yang, W. Ren, X. Zheng, S. Meng, C. Cai, X. Fu, S. Chen, *ACS Appl. Mater. Interfaces* **2022**, *14*, 54649–54661.
37 T. Xia, W. Gong, Y. Chen, M. Duan, J. Ma, X. Cui, Y. Dai, C. Gao, Y. Xiong, *Angew. Chem. Int.* Ed. **2022**, *61*, 202204225−202204230
38 Y.-H. Li, F. Zhang, Y. Chen, J.-Y. Li, Y.-J. Xu, *Green Chem.* **2020**, *22*, 163–169.
39 C.-L. Tan, M.-Y. Qi, Z.-R. Tang, Y.-J. Xu, *Appl. Catal., B* **2021**, *298*, 120541–120549.
40 L. Sun, W. Wang, T. Kong, H. Jiang, H. Tang, Q. Liu, *J. Mater. Chem. A* **2022**, *10*, 22531–22539.